Article

Current Biology

In *trans* neuregulin3-Caspr3 interaction controls DA axonal bassoon cluster development

Graphical abstract

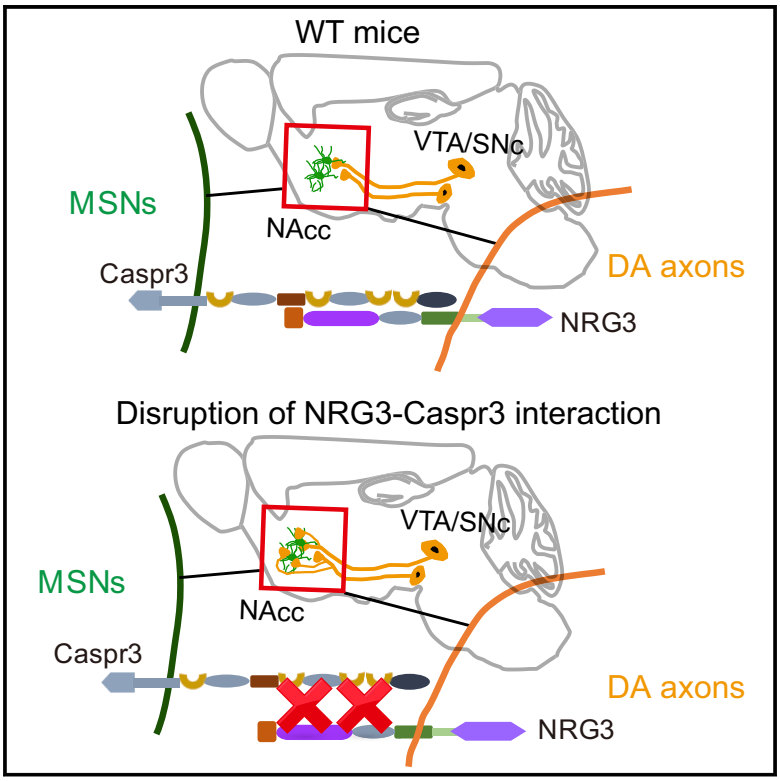

Highlights

- Correlation of NRG3 with DA axonal bassoon clusters during development
- Ablation of NRG3 increased DA axonal bassoon clusters and DA transmission
- Caspr3 interacts in *trans* with NRG3 in the striatum
- Disruption of the NRG3-Caspr3 interaction increased DA bassoon clusters on MSNs

Authors

Wanpeng Cui, Nannan Gao, Zhaoqi Dong, ..., Heath Robinson, Wen-Cheng Xiong, Lin Mei

Correspondence

lin.mei@case.edu

In brief

Cui et al. show that Neuregulin3 in dopaminergic neurons interacts with Caspr3 from medium spiny neurons in *trans* and controls the development of dopaminergic axonal bassoon clusters. Disruption of this NRG3-Caspr3 interaction increases dopamine release and impairs the behaviors related to dopaminergic transmission.

Cui et al., 2021, Current Biology *31*, 1–13
August 9, 2021
https://doi.org/10.1016/j.cub.2021.05.045

CellPress

Please cite this article in press as: Cui et al., In *trans* neuregulin3-Caspr3 interaction controls DA axonal bassoon cluster development, Current Biology (2021), https://doi.org/10.1016/j.cub.2021.05.045

Current Biology

CellPress

Article

In *trans* neuregulin3-Caspr3 interaction controls DA axonal bassoon cluster development

Wanpeng Cui,[1,5] Nannan Gao,[1,5] Zhaoqi Dong,[1] Chen Shen,[1] Hongsheng Zhang,[1] Bin Luo,[1] Peng Chen,[1] Davide Comoletti,[3,4] Hongyang Jing,[1] Hongsheng Wang,[1] Heath Robinson,[1] Wen-Cheng Xiong,[1,2] and Lin Mei[1,2,6,*]

[1]Department of Neurosciences, School of Medicine, Case Western Reserve University, 10900 Euclid Avenue, Cleveland, OH 44106, USA
[2]Louis Stokes Cleveland Veterans Affairs Medical Center, Cleveland, OH 44106, USA
[3]School of Biological Sciences, Victoria University of Wellington, Wellington 6140, New Zealand
[4]Child Health Institute of New Jersey, and Departments of Neuroscience and Cell Biology, Robert Wood Johnson Medical School, Rutgers University, New Brunswick, NJ 08901, USA
[5]These authors contributed equally
[6]Lead contact
*Correspondence: lin.mei@case.edu
https://doi.org/10.1016/j.cub.2021.05.045

SUMMARY

Dopamine (DA) transmission is critical to motivation, movement, and emotion. Unlike glutamatergic and GABAergic synapses, the development of DA synapses is less understood. We show that bassoon (BSN) clusters along DA axons in the core of nucleus accumbens (NAcc) were increased in neonatal stages and reduced afterward, suggesting DA synapse elimination. Remarkably, DA neuron-specific ablating neuregulin 3 (NRG3), a protein whose levels correlate with BSN clusters, increased the clusters and impaired DA release and behaviors related to DA transmission. An unbiased screen of transmembrane proteins with the extracellular domain (ECD) of NRG3 identified Caspr3 (contactin associate-like protein 3) as a binding partner. Caspr3 was enriched in striatal medium spiny neurons (MSNs). NRG3 and Caspr3 interact in *trans*, which was blocked by Caspr3-ECD. Caspr3 null mice displayed phenotypes similar to those in DAT-*Nrg3*$^{f/f}$ mice in DA axonal BSN clusters and DA transmission. Finally, *in vivo* disruption of the NRG3-Caspr3 interaction increased BSN clusters. Together, these results demonstrate that DA synapse development is controlled by *trans* interaction between NRG3 in DA neurons and Caspr3 in MSNs, identifying a novel pair of cell adhesion molecules for brain circuit wiring.

INTRODUCTION

Functional circuits are generated and refined by synapse formation and synapse elimination during development. In the critical period, a surplus of synapses are made, and excess synapses must be eliminated to establish neuronal circuits with high specificity.[1–3] Midbrain dopaminergic (DA) neurons project to the striatum (nigrostriatal and mesolimbic pathway) and prefrontal cortex (mesocortical pathway), and regulate movement-related activities, reinforcement learning, and motivation.[4–7] DA transients are frequently associated with physiological responses such as reward processing, social interaction, and drug addiction.[8–11] Abnormal DA circuits and transmission (in particular phasic transmission) are implicated in neurodevelopmental disorders such as schizophrenia (SZ), attention deficit hyperactivity disorder (ADHD), and major depression.[12–15] Medium spiny neurons (MSNs) in the striatum receive inputs from midbrain DA neurons that innervate on their dendritic shafts (axondendritic synapses) or neck of the spine (axospinous synapses).[16,17] In neonatal stages of rodents, DA efferent axons aggregate in the striosomes of the striatum but also form synapses in the matrix.[18,19] DA synapses in both regions increased initially but reduced in late stages.[19] The density of DA synapses in the striatum of adult mice is around 1 synapse per 10 μm^3, accounting for ~21% of total synapses in mouse striatum.[20,21] About 20% of them are functionally active in releasing DA while the rest of the DA vesicle-containing varicosities in the striatum are silent synapses.[22] However, mechanisms of DA synapse development are not well understood. This process could be regulated by cell adhesion molecules that bidirectionally coordinate the structure and function of pre- and post-synaptic terminals.[23] For example, neuroligin2 (NLGN2) and neurexin are implicated in forming DA synapses onto GABAergic postsynaptic structures.[24]

DA neurons form dense innervation in the striatum, which makes it difficult to study their development *in vivo*.[25] To this end, we analyzed DA axonal BSN clusters by super-resolution imaging of expanded striatum using the magnified analysis of the proteome (MAP).[26] We found that DA axonal BSN clusters in the nucleus accumbens (NAcc) are tightly regulated in the postnatal period. We screened for molecules whose expression correlates with BSN clusters and identified NRG3, a transmembrane trophic factor of the NRG family that binds and activates the receptor tyrosine kinase, ErbB4 (ErbB2 receptor tyrosine kinase 4).[27] NRG3 also regulates glutamate release from pyramidal neurons.[28] To understand the function of NRG3 in DA

Please cite this article in press as: Cui et al., In *trans* neuregulin3-Caspr3 interaction controls DA axonal bassoon cluster development, Current Biology (2021), https://doi.org/10.1016/j.cub.2021.05.045

neurons, we generated mice that lack NRG3 specifically in DA neurons. We found that NRG3 deletion in DA neurons increased the number of DA axonal BSN clusters in the NAcc, indicating that NRG3 may play a role in limiting the number of DA synapses. The mutation caused hyperactivity, increased preference in cocaine-induced place preference (CPP), and impaired working memory and social behaviors. We found that NRG3 interacts with Caspr3 via the extracellular domain. The number of DA axonal BSN clusters and/or potentiation of DA transmission was increased by Caspr3 mutation or by disrupting the interaction with NRG3. These results demonstrate that NRG3 interacts with Caspr3 in *trans* to control DA synapse development.

RESULTS

Neonatal DA axonal BSN clusters and increased NRG3 expression in neonatal VTA DA neurons

We analyzed developing BSN clusters along DA axons from the ventral tegmental area (VTA) onto MSNs in the striatum by MAP, a method that expands brain tissues. MAP enabled 3.5- to 4-fold linear expansion of the striatal tissue (Figures 1A, 1B, and S1A). DA axonal BSN clusters were defined as TH+ axons that co-stained with BSN[29] and were quantified after 3D reconstruction (Figures S1B and S1C). They appeared in aggregates in the DA islands before postnatal day 10 (P10) (Figure S1E). The density of BSN+TH+ puncta in the striatum was increased from P0 to P10 and reduced afterward (Figures 1C and 1D), consistent with an early study.[19] Thus, more DA synapses were formed in the striatum during development and were later eliminated. To investigate underlying mechanisms, we screened for cell adhesion molecules that are implicated in synapse development. VTA and substantia nigra pars compacta (VTA/SNc) were isolated from *DAT*::*Cre*;*Ai14* mice (Figure 1E); qRT-PCR analysis revealed that NRG3 mRNA was around 8-fold higher at P3 than that of P60 mice (Figure 1F). NRG3 increase was confirmed by patch-seq (Figures 1G and 1H) and western analysis (Figure 1M). *In situ* hybridization indicated that *Nrg3* mRNA was present in ~99% of TH+ neurons in the VTA/SNc region (Figures 1I–1L). The time courses of NRG3 protein and DA axonal BSN clusters overlapped (Figure 1N). Subcellularly, NRG3 was detectable in TH+ DA axons in NAcc (Figure S1D). Together, these results demonstrate that NRG3 expression in DA neurons correlates with DA axonal BSN clusters, suggesting a role of NRG3 in DA synapse development.

Increased DA axonal BSN clusters in DAT-*Nrg3*$^{f/f}$ mice

To test the hypothesis, we deleted Nrg3 in DA neurons by using *DAT*::*Cre* mice that express Cre in DA neurons (Figure S1F). *DAT*::*Cre*; *Nrg3*$^{f/f}$ mice (hereafter referred to as DAT-*Nrg3*$^{f/f}$) showed undetectable *Nrg3* mRNA in DA neurons (Figure S1I) or NRG3 protein in the VTA/SNc region, where DA neuronal somas are concentrated, unlike control (i.e., *Nrg3*$^{f/f}$ hereafter) mice. NRG3 was also reduced in efferent regions such as NAcc and DS, suggesting a reduction in DA axons. NRG3 in the prefrontal cortex (PFC), another efferent region that is less innervated by DA axons, showed a trend of reduction (Figures S1G and S1H). These results indicate that NRG3 was reduced in DA neuronal somas and axons. TH levels and TH+ DA neurons in VTA/SNc were similar between the two genotypes (Figures 2A–2D and S2J), indicating that NRG3 deletion did not alter the number of DA neurons. It did not change TH intensity of the medial forebrain bundle (MFB), suggesting similar numbers of DA axons in the bundle (Figures S2D–S2F). However, TH levels was elevated in efferent target regions including PFC, NAc, and DS in DAT-*Nrg3*$^{f/f}$ mice (Figures 2A, 2B, and S2G–S2I). Results indicate increased TH+ axonal branches in PFC and ventral NAcc (Figures 2E–2H). Immuno-electron microscopic (EM) analysis showed increased TH+ axons in NAcc in DAT-*Nrg3*$^{f/f}$ mice, compared with *Nrg3*$^{f/f}$ control (Figures S2O and S2P). Note that TH+ DA axons were positive for vesicular monoamine transporter2 (VMAT2), a marker of DA-containing vesicles, and TH+ VMAT2+ axons increased in mutant mice (Figures S2A–S2C). Together, these results suggest extensive DA axon terminal arborization in Nrg3 mutant mice.

Next, we determined whether Nrg3 mutation altered the number of DA axonal BSN clusters by super-resolution imaging. In control mice, the number of DA axonal BSN clusters peaked at P10 and reduced at P60 (Figures 1D and 2K). The BSN clusters were similar between mutant and control mice at P0 and P10 (including both the striosome and matrix region), suggesting that NRG3 is not necessary for DA synapse formation (Figures S2K–S2N). However, they remained higher in P60 DAT-*Nrg3*$^{f/f}$ mice, compared with control mice, suggesting that NRG3 may be necessary for maturation or eliminating DA synapse (Figures 2I and 2J). However, virally expressing NRG3 in VTA in P0 mice has no effect on BSN clusters at P30 (Figures S2Q–S2W). These results identify a critical role of NRG3 in controlling the number of DA synapses in efferent target regions of midbrain DA neurons.

Increased DA transmission of DAT-*Nrg3*$^{f/f}$ mice

Spontaneous DA transients result from the synchronized activity of DA neurons and are associated with reward and learning behaviors.[9,30] To characterize the function of DA axonal BSN clusters, we recorded DA transients in ventral NAcc *in vivo* by fast-scanning cyclic voltammetry (FSCV) recordings. The criteria of qualified DA transients were 3 times the standard deviation (SD) above the baseline with a peak higher than 5 nM of DA, and with a voltammogram of DA.[31,32] The number and amplitude of transients were significantly increased in DAT-*Nrg3*$^{f/f}$ mice (Figures 3A–3D, 3M, and 3N). Notice that these transients were potentiated dose-dependently by raclopride, a D2 receptor (D2R) antagonist (Figures 3E–3N).[33] DA release is regulated by cholinergic transmission in NAc mainly via β2-AChR.[34–36] In the presence of dihydro-b-erythroidine (DHβE), an antagonist of β2-AChR, evoked DA release was higher in DAT-*Nrg3*$^{f/f}$ slices, compared with control slices (Figures 3O and 3P), suggesting that DA release increase in mutant mice does not depend on cholinergic transmission. In addition, DA, but not 5-HT, levels in the striatum were increased in DAT-*Nrg3*$^{f/f}$ mice, compared with control mice (Figures 3Q and 3R). Together, these results revealed increased DA transmission in ventral NAcc by deleting Nrg3 in DA neurons. By characterizing DA neurons in the parabrachial pigmented nucleus of the VTA (PBP) in slices, we showed that Nrg3 mutation did not alter the resting membrane potential or the input resistance (Figures S3A and S3B) or the number of action potentials and interspike intervals (ISIs) in response to injected currents (Figures 3S–3U). By single-unit recording *in vivo*, we found that Nrg3 mutation had little effect

Please cite this article in press as: Cui et al., In *trans* neuregulin3-Caspr3 interaction controls DA axonal bassoon cluster development, Current Biology (2021), https://doi.org/10.1016/j.cub.2021.05.045

CellPress

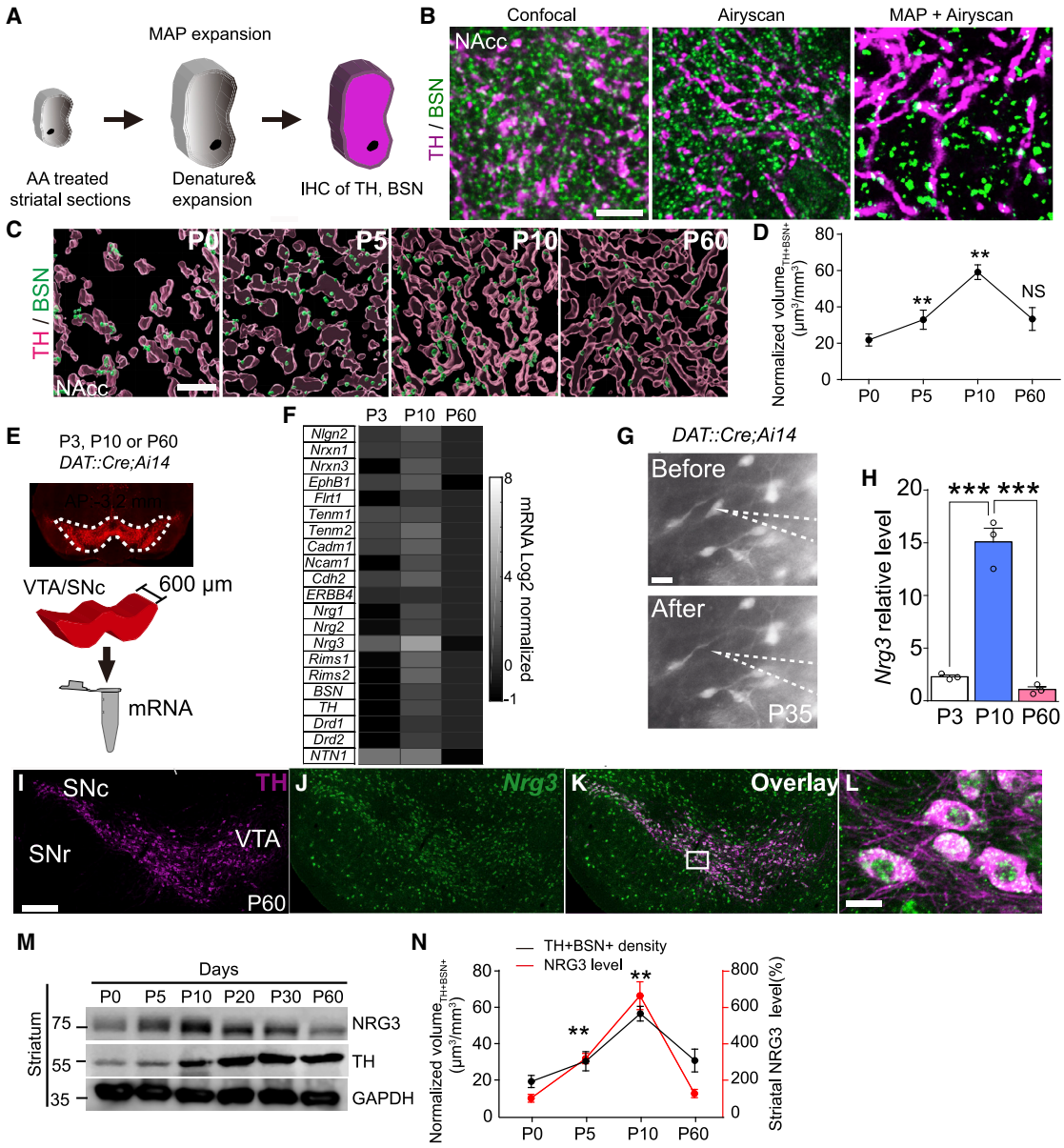

Figure 1. Identification of NRG3 as a key molecule in DA axonal BSN cluster development during the critical period

(A) Schematic diagram showing tissue expansion using MAP in the striatum.

(B) MAP and airyscan increased the resolution in the striatum analysis of TH/BSN clusters. TH (DA axons, magenta) and BSN (green). Scale bar, 5 μm.

(C and D) The density of DA axonal BSN clusters in NAcc was increased in neonatal stages (P0–P10) and decreased afterward (P60). Scale bar, 7 μm.

(C) Representative images.

(D) Quantification of (C). n = 3 mice for each group. **p < 0.01, $F_{(3,16)} = 37.89$.

(E) Schematic workflow of screening critical cell adhesion molecules.

(F) Heatmap represents the mRNA levels of cell adhesion molecules in different postnatal stages from VTA/SNc. n = 3 mice for each developmental stage.

(G) Representative images showing an example of a DA neuron isolated from a midbrain slice before (upper panel) and after (lower panel) patch. Scale bar, 20 μm.

(H) Quantification of *Nrg3* mRNA at P10. n = 3 mice for each group. ***p < 0.001, $F_{(2,6)} = 99.71$. Data are mean ± SEM. One-way ANOVA followed by Tukey's post hoc.

(I–L) Coronal section through the midbrain of P60 mouse showing the co-localization of *Nrg3* mRNA (green in J–L) with TH (red in I, K, and L). (L) Enlarged rectangle area in red rectangle area of (K). Scale bar, 200 μm (I) and 10 μm (L).

(M) Developmental changes of NRG3 and TH proteins by western blotting.

(N) Quantification of (M). Data represent mean ± SEM. **p < 0.01. $F_{(3.8)} = 106.1$.

Data are mean ± SEM. One-way ANOVA followed by Tukey's post hoc. See also Figure S1 and Table S1.

Please cite this article in press as: Cui et al., In *trans* neuregulin3-Caspr3 interaction controls DA axonal bassoon cluster development, Current Biology (2021), https://doi.org/10.1016/j.cub.2021.05.045

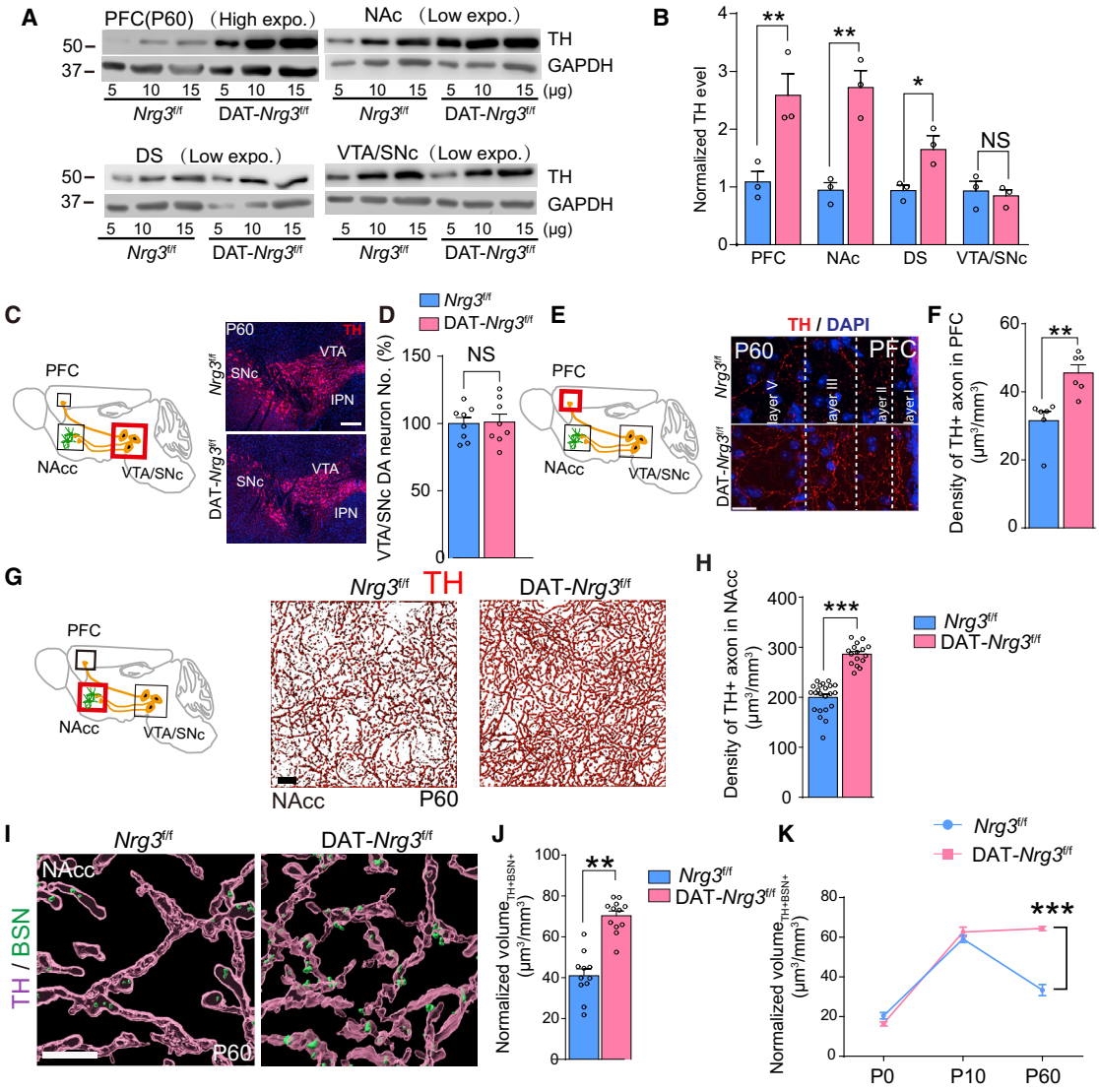

Figure 2. Increased DA axonal BSN clusters in DAT-*Nrg3*$^{f/f}$ mice

(A and B) TH proteins in different regions of indicated mice.

(A) Representative blots of TH and GAPDH from PFC, NAc, DS, and VTA/SNc of *Nrg3*$^{f/f}$ and DAT-*Nrg3*$^{f/f}$ mice.

(B) Quantification of (A).

Two-way ANOVA with Sidak's post hoc. Effect of genotype, $F_{(1,16)} = 47.91$, $p < 0.0001$. n = 3 for each group. NS, not significant. $^{**}p < 0.01$, $^{*}p < 0.05$.

(C and D) No change in the number of DA neurons in DAT-*Nrg3*$^{f/f}$ mice.

(C) Schematic diagram showing DA neurons in VTA/SNc (left). Scale bar, 200 μm.

(D) Quantification of (C). p = 0.8859, Student's t test, t = 0.1461, n = 8 mice for each group.

(E) Coronal sections showing increased TH+ DA axons in the prelimbic cortex (Prl) of DAT-*Nrg3*$^{f/f}$ mice. Right: representative TH staining in PFC. Scale bar, 20 μm.

(F) Quantification of (E). p = 0.0031, Student's t test, t = 3.875, n = 6 mice for each group. $^{**}p < 0.01$.

(G and H) Increased TH+ axons in NAcc in P60 DAT-*Nrg3*$^{f/f}$ mice.

(G) Representative 3D surface reconstruction images. TH+ axons in NAcc of both groups (middle and right). Scale bar, 5 μm.

(H) Quantification of (G). $^{***}p < 0.0001$, Student's t test, t = 9.947, n = 4 mice for each group.

(I and J) Increased TH+ BSN clusters in DAT-*Nrg3*$^{f/f}$ mice.

(I) Representative 3D images of TH+ (purple) DA axons and BSN clusters (green). Scale bar, 1 μm.

(J) Quantification of (I). $p < 0.001$, Student's t test, t = 7.287, n = 11–12 slices from 4 mice for each group.

(K) Developmental changes of TH+BSN+ clusters. $^{***}p < 0.001$, two-way ANOVA with Sidak's post hoc. Effect of genotype interaction, $F_{(1, 24)} = 45.04$, $p < 0.0001$.

Data are mean ± SEM.

See also Figure S2.

Please cite this article in press as: Cui et al., In *trans* neuregulin3-Caspr3 interaction controls DA axonal bassoon cluster development, Current Biology (2021), https://doi.org/10.1016/j.cub.2021.05.045

CellPress

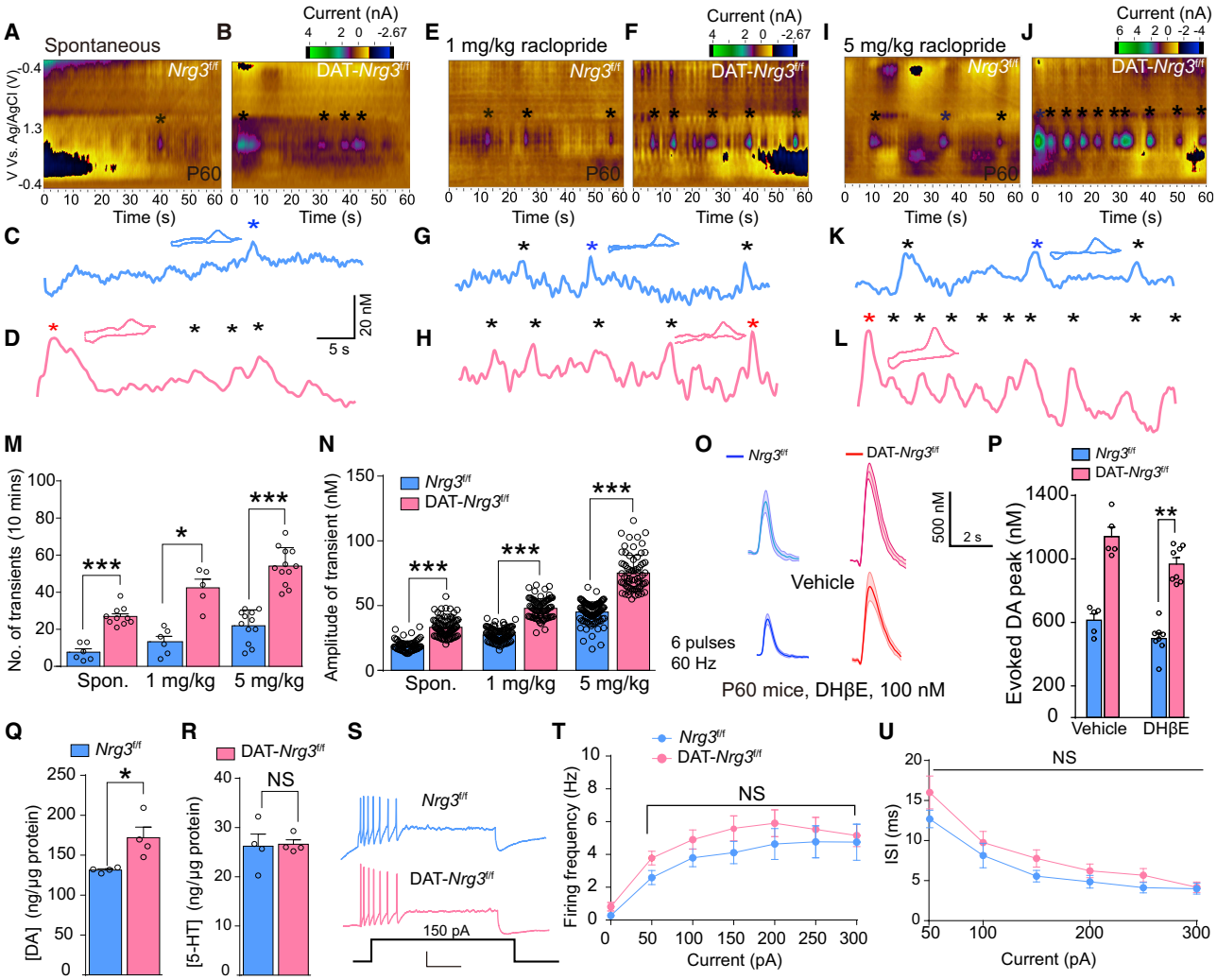

Figure 3. Increased DA transmission in DAT-*Nrg3*$^{f/f}$ mice

(A–D) Increased spontaneous DA transients in DAT-*Nrg3*$^{f/f}$ mice.

(A and B) Heatmap of FSCV. Asterisks, DA transients.

(C and D) Plots of DA concentration versus time plotting in the spontaneous condition. Insets: voltammograms of DA. Scale bars, 5 s, 20 nM (D).

(E and F) Potentiation of DA transients by 1 mg/kg raclopride (i.p.) in DAT-*Nrg3*$^{f/f}$ mice.

(G and H) Plots of DA concentration versus time plotting under 1 mg/kg raclopride.

(I and J) Increased DA transients after 5 mg/kg raclopride (i.p.) in DAT-*Nrg3*$^{f/f}$ mice.

(K and L) Plots of DA concentration versus time plotting under 5 mg/kg raclopride.

(M) Increased number of DA transients in DAT-*Nrg3*$^{f/f}$ mice. Two-way ANOVA. Effect of genotype, $F_{(1.47)} = 136.9$, $p < 0.001$, followed by Sidak's post hoc. ***$p < 0.001$, *$p < 0.05$.

(N) Increased amplitudes of DA transients in DAT-*Nrg3*$^{f/f}$ mice. $F_{(1, 520)} = 976.7$, $p < 0.0001$. n = 10–12 mice for each genotype. Two-way ANOVA followed by Sidak's post hoc. ***$p < 0.001$.

(O) Electrical stimulation evoked a larger peak of DA in brain slices from DAT-*Nrg3*$^{f/f}$ mice. 100 nM DHβE. Scale bar, 500 nM, 2 s.

(P) Quantification of (O). $F_{(3,22)} = 47.810$, $p < 0.001$, one-way ANOVA with Sidak's post hoc. n = 8 slices from 3 mice for DHβE group. **$p < 0.01$.

(Q) Increased striatal DA level in DAT-*Nrg3*$^{f/f}$ mice detected by LC-MS. *Nrg3*$^{f/f}$ (131.4 ± 1.587), n = 4 versus DAT-*Nrg3*$^{f/f}$ mice (171.9 ± 13.29 ng/μg), n = 4, t = 3.027, p = 0.0232.

(R) No difference in striatal 5-HT level. t = 0.1478, p = 0.8874, Student's t test.

(S–U) No difference in excitability in brain slice preparation.

(S) Example action potential traces from VTA-DA neurons. Scale bar, 25 mV, 500 ms.

(T) Quantification of firing rates. n = 22 neurons from 3 *DAT::Cre*;*Ai14* mice, n = 16 neurons from 3 DAT-*Nrg3*$^{f/f}$; *Ai14* mice. Effect of genotype interaction, $F_{(1,36)} = 1.262$, p = 0.2687. Effect of current, $F_{(6, 216)} = 28.55$, $p < 0.0001$. Genotype × current interaction, $F_{(6, 216)} = 0.3985$, p = 0.8795.

(U) Quantification of ISI. n = 22 neurons from 3 *DAT::Cre*;*Ai14* mice, n = 16 neurons from 3 DAT-*Nrg3*$^{f/f}$; *Ai14* mice. Genotype × current interaction, $F_{(5, 155)} = 0.7552$, p = 0.5835. Effect of genotype interaction, $F_{(1,31)} = 2.350$, p = 0.1354. Effect of current, $F_{(5, 155)} = 40.88$, $p < 0.0001$. Two-way ANOVA with Sidak's post hoc. See also Figure S3.

Please cite this article in press as: Cui et al., In *trans* neuregulin3-Caspr3 interaction controls DA axonal bassoon cluster development, Current Biology (2021), https://doi.org/10.1016/j.cub.2021.05.045

on firing patterns, frequency, or ISI of DA neurons or the percentage of bursty firing DA neurons (Figures S3C–S3G). Together, these results indicate that Nrg3 mutation increases DA transmission by maintaining more DA axon terminals and synapses without changing DA neuron-intrinsic property.

DA-related behavioral deficits of NRG3 mutant mice

To determine whether dysregulated DA transmission alters behaviors, mice were subjected to a battery of behavioral tests. First, in the open field, compared with control mice, DAT-*Nrg3*$^{f/f}$ mice showed an increase in total distance, but not in time spent in the central arena (Figures 4A–4C), suggesting increased locomotor activity. Second, we performed a CPP test where mice were conditioned with cocaine (10 mg/kg, i.p. [intraperitoneally]) in one of the two chambers. Prior to cocaine conditioning, both *Nrg3*$^{f/f}$ and DAT-*Nrg3*$^{f/f}$ mice did not show any preference for either chamber (Figures 4D and 4E), suggesting little effect of hyperactivity or chamber preference. However, after cocaine conditioning, DAT-*Nrg3*$^{f/f}$ mice displayed increased preference scores for the cocaine-paired chamber (Figures 4F–4H). These results suggest that Nrg3 mutation sensitized mice to cocaine, consistent with hyperactive DA transmission. Third, Nrg3 mutation reduced spontaneous alteration ratio in Y-maze (Figures 4I and 4J) but had no effect on arm entries (Figure 4K), suggesting an impairment of working memory. Finally, in three-chamber social interaction tests, DAT-*Nrg3*$^{f/f}$ mice exhibited normal sociability and social novelty behavior (Figures 4L–4N). However, the social interaction index from the sociability test was reduced in DAT-*Nrg3*$^{f/f}$ mice (Figure 4O), suggesting impaired social preference. Collectively, these results demonstrate that DAT-*Nrg3*$^{f/f}$ mice are impaired in DA-related behaviors.

Caspr3 interaction in *trans* with NRG3

NRG3 is a ligand that binds to and activates ErbB4;[37] however, ErbB4 activation has been implicated to increase DA transmission.[38] ErbB4 null mutation seemed to have little effect on DA axonal BSN clusters and axon branches in NAcc (Figures S4A–S4D). These observations suggest that NRG3 regulates DA synapses and transmission in an ErbB4-independent mechanism. We speculated that NRG3 may interact in *trans* with a transmembrane protein of MSNs. To this end, NRG3-ECD was fused with alkaline phosphatase (AP) (NRG3-ECD-AP) and used as a bait to screen for a library of ~400 transmembrane proteins (Figure 5A). This assay is highly sensitive since it uses a novel strategy to tetramerize bait and prey proteins.[39,40] The screens identified ErbB4, which validates the method, and a novel protein, Caspr3 (Figure 5B; Tables S2 and S3). When NRG3-ECD-AP and Caspr3-ECD-Fc recombinant proteins were mixed, NRG3-ECD was detected in the precipitates with anti-Caspr3 antibody (Figure 5C), confirming the interaction. NRG3 was detected in Caspr3 precipitates from *Nrg3*$^{f/f}$ striatal homogenates (Figure 5D), suggesting that the interaction occurs *in vivo*. The interaction with NRG3 involved LamG1 and LamG2, two EGF domains, in the ECD of Caspr3 (Figures S5D and 5E).[41] These results suggest that NRG3 interacts with Caspr3 in the striatum, likely via LamG1 and LamG2 of Caspr3.

Next, we determined whether NRG3 and Caspr3 interact in *trans* by cell aggregation assay. As a positive control, aggregates formed when cells transfected with Neuroligin2 (with GFP) were mixed with those with Neurexin1β (with RFP) (Figures 5F and 5G). Aggregates were also increased when Caspr3-expressing cells were mixed with NRG3-expressing cells (Figure 5H). Importantly, the addition of recombinant Caspr3-ECD reduced cell aggregates (Figure 5I). These results identify Caspr3 as a novel binding partner that could mediate in *trans* interaction with NRG3.

Similar phenotypes of Caspr3 mutant mice

Immunostaining of coronal sections with anti-Caspr3 antibody revealed high-intensity staining in the striatum (Figure 6A). Similarly, levels of Caspr3 were high in NAc and DS where MSN somas are concentrated, but relatively low in VTA/SNc and PFC (Figures 6B and 6C). Caspr3 was not detectable in staining or western analysis of Caspr3 null (Caspr3$^{-/-}$) samples, indicative of antibody specificity (Figures S6A–S6C, 6A, and 6B). These results indicate that Caspr3 is enriched in regions where MSN somas are located. We noticed that Caspr3 appeared to be at a higher level in medial regions of the striatum (Figure 6A), the dorsal medial quadrant of the striatum, and medial NAc than in lateral quadrants (Figures 6E and 6F). Co-staining with DAPAR32, a marker of MSNs, revealed that 90.1% Caspr3+ cells are MSNs whereas almost all MSNs were Caspr3+ (Figures S6C and S6D). To determine the subcellular localization of Caspr3, GFP was iontoporated into NAc of P0 mice to label MSNs.[42] Striatal sections of P40 mice were stained with anti-Caspr3 and anti-DARPP32 antibodies. Caspr3 puncta were observed in both the soma and dendritic shafts of GFP-labeled MSNs (Figures S6E and S6F).

To study the function of Caspr3, we first analyzed TH levels in VTA/SNc and efferent target regions of Caspr3$^{-/-}$ mice. TH levels were increased in efferent target regions such as NAc and DS in P60 Caspr3$^{-/-}$ mice (Figures 6B and 6D), a phenotype also seen in DAT-*Nrg3*$^{f/f}$ mice. However, TH levels in VTA/SNc were similar between the two genotypes. Like DAT-*Nrg3*$^{f/f}$ mice, Caspr3$^{-/-}$ mice showed no change in the number of DA neurons (Figures 6G–6I). 3D reconstruction indicated an increase in TH+ axon density in ventral NAcc of Caspr3$^{-/-}$ mice (Figures 6J–6L), suggesting an increased DA axonal arborization. Moreover, the density of BSN+ puncta in TH+ in the ventral NAcc was increased in Caspr3$^{-/-}$ mice, compared with control mice (Figures 6M and 6N). These results suggest an increase in DA synapses in efferent target regions of midbrain DA neurons. Caspr3 mutation increased the number and amplitude of transients, which could be potentiated by raclopride (Figures S7A–S7H) and DA release in the presence of DHβE (Figures S7I and S7J). The similarity of phenotypes of DAT-*Nrg3*$^{f/f}$ mice and Caspr3$^{-/-}$ mice supports the notion that the two molecules act in the same or related pathway to regulate developing DA circuits.

A role of the NRG3-Caspr3 interaction for proper DA synapses

The above results support a working model that presynaptic NRG3 interacts with Caspr3 in *trans* to prevent overformation of DA synapses onto MSNs. To test this hypothesis, we sought to disrupt the NRG3-Caspr3 interaction *in vivo* by Caspr3-ECD. It was detected in the culture medium of transfected HEK293 cells (Figure 5C) and could attenuate the aggregation of HEK293 cells expressing NRG3 and Caspr3, respectively (Figures 5I and 5J). Bilateral striatum of P0 mice was co-iontoporated with GFP without or with Caspr3-ECD plasmid with TCHD

Please cite this article in press as: Cui et al., In *trans* neuregulin3-Caspr3 interaction controls DA axonal bassoon cluster development, Current Biology (2021), https://doi.org/10.1016/j.cub.2021.05.045

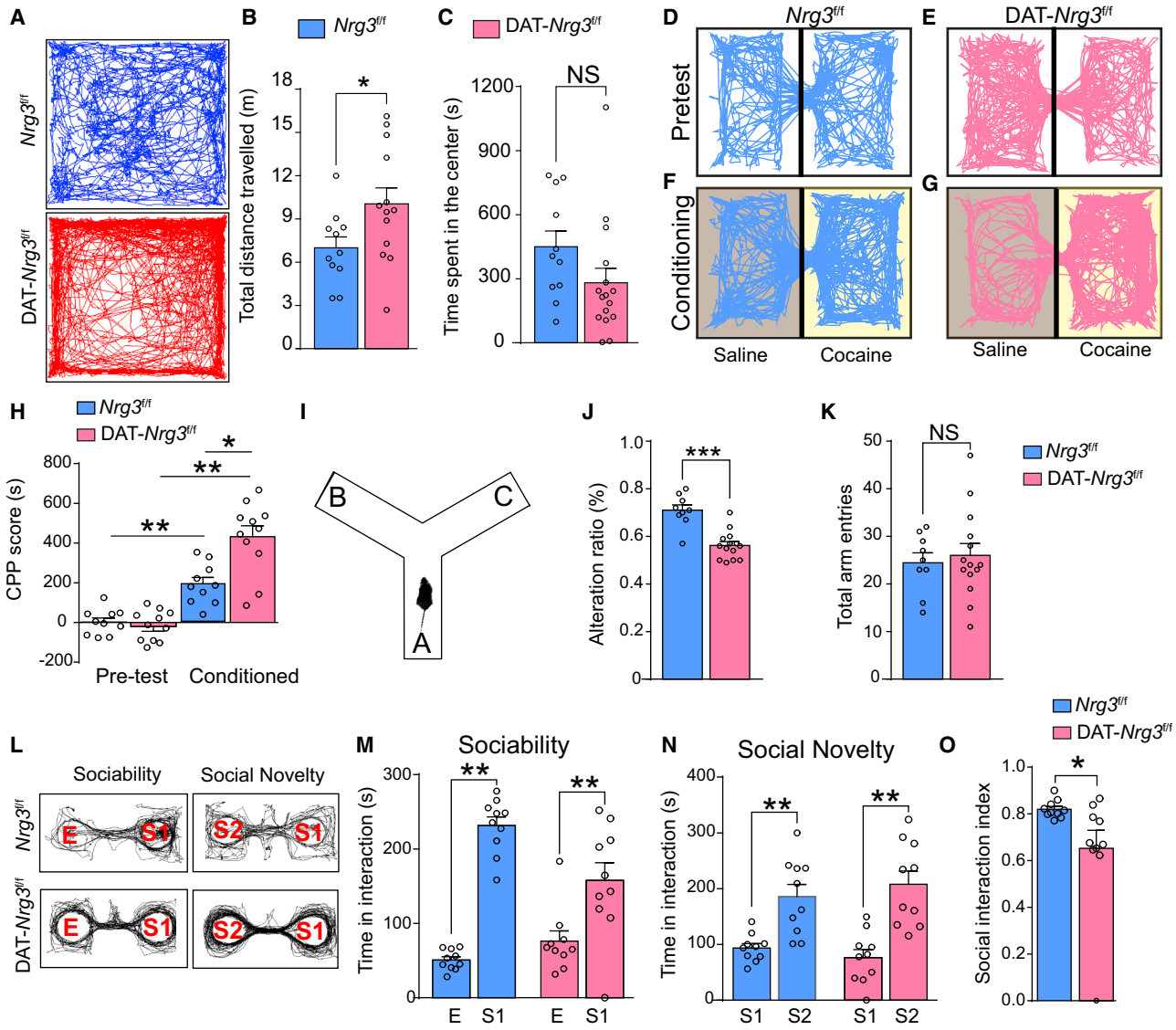

Figure 4. Loss of NRG3 in DA neurons leads to behavioral deficits related to DA transmission

(A–C) Hyperlocomotion in open field.

(A) Traces of both genotypes.

(B) Total distance traveled. n = 11 from *Nrg3*$^{f/f}$ mice, n = 13 from DAT-*Nrg3*$^{f/f}$ mice. p = 0.0393, t = 2.192.

(C) Time spent in the center. n = 11 from *Nrg3*$^{f/f}$ mice, n = 16 from DAT-*Nrg3*$^{f/f}$ mice. p = 0.1120, t = 1.648, Student's t test.

(D–H) Increased CPP scores in DAT-*Nrg3*$^{f/f}$ mice. (D–G) Representative traces of mice in CPP. (F and G) Brown, chambers paired with saline; yellow, chambers paired with 10 mg/kg cocaine. (H) Quantification. *Nrg3*$^{f/f}$ versus DAT-*Nrg3*$^{f/f}$ mice, p = 0.9748. After CPP, *Nrg3*$^{f/f}$ versus DAT-*Nrg3*$^{f/f}$ mice, p = 0.0003, $F_{(3.38)}$ = 33.7684. n = 10 for *Nrg3*$^{f/f}$ mice and n = 11 for DAT-*Nrg3*$^{f/f}$ mice. One-way ANOVA followed by Tukey's post hoc.

(I–K) Impaired spatial-working memory in DAT-*Nrg3*$^{f/f}$ mice tested in Y-maze.

(I) Schematic diagram of Y-maze test.

(J) Reduced spontaneous alteration ratio in DAT-*Nrg3*$^{f/f}$ mice. p < 0.001, t = 5.564.

(K) No difference in the total arm entries. p = 0.112, t = 1.648, Student's t test. n = 9 for *Nrg3*$^{f/f}$ and n = 11 for DAT-*Nrg3*$^{f/f}$ group.

(L) Representative traces in the sociability (left) and social novelty tests (right).

(M and N) Normal sociability (M) and social novelty (N). Sociability, $F_{(1.36)}$ = 2.587, p = 0.1165. Social novelty, $F_{(1.36)}$ = 0.014, p = 0.9036. n = 10 for *Nrg3*$^{f/f}$ and DAT-*Nrg3*$^{f/f}$ mice. Two-way ANOVA followed by Sidak's post hoc.

(O) Decreased social interaction index in sociability in DAT-*Nrg3*$^{f/f}$ mice. p = 0.0466, t = 2.136, Student's t test. Bar graph, mean ± SEM. n = 10 for *Nrg3*$^{f/f}$ and DAT-*Nrg3*$^{f/f}$ mice.

*p < 0.05, **p < 0.01, ***p < 0.001; NS, not significant.

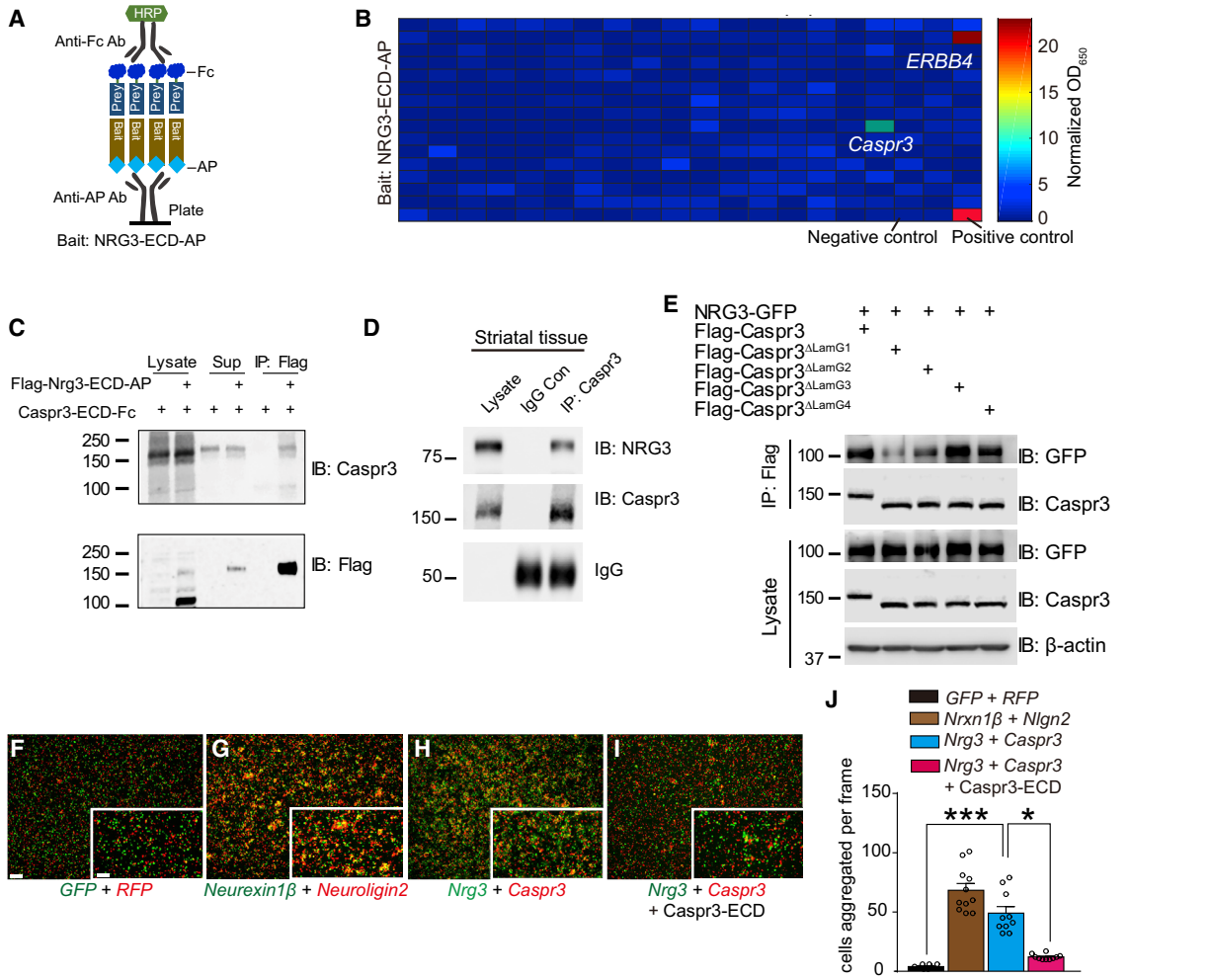

Figure 5. Caspr3 interaction in *trans* with NRG3

(A) Schematic diagram indicates the interaction of NRG3-ECD binding with candidate partners in an ELISA-based screening.

(B) Identification of ErbB4 and Caspr3 as binding partners of NRG3.

(C) NRG3-ECD interacts with the Caspr3-ECD in co-immunoprecipitation (coIP) using HEK293 cells.

(D) Association of Caspr3-NRG3 *in vivo*. CoIP of Caspr3 and NRG3 using mouse striatal tissue from $Nrg3^{f/f}$ mice.

(E) NRG3 binds to the LamG1 and LamG2 domain of Caspr3.

(F–I) NRG3 and Caspr3 interaction in *trans*, and Caspr3-ECD blocked NRG3-Caspr3 interaction *in vitro*. Insets are high magnification. Scale bars, 200 μm (F) and 100 μm (inset).

(J) Quantification of aggregated cells in (F)–(I). *Nrxn1β* + *Nlgn2* (68.36 ± 18.76), pCDNA3.0 + pCDNA3.0 (4.00 ± 1.73), *Nrg3* + *Caspr3* (49.1 ± 17.45), *Nrg3* + *Caspr3*+Caspr3-ECD (12.10 ± 2.33). $F_{(3,35)} = 50.0$, n = 11 frames for *Nrxn1β* + *Nlgn2* group, n = 10 for *NRG3* + *Caspr3*, n = 8 frames for *GFP* + *RFP*, n = 10 for *NRG3* + *Caspr3*+Caspr3-ECD. *p < 0.05. Data are mean ± SEM. Two-way ANOVA with Sidak's post hoc.

See also Figure S4 and Tables S2 and S3.

(trans-cyclohexane-1,2-diol), which helps genome incorporation.[42] GFP was detected in neurons in the striatum as early as ~12 h after surgery (Figures 7B and 7C). 72.2% of GFP-positive cells were labeled by DARPP32, suggesting that they were MSNs (Figures 7D and 7E). Caspr3-ECD was detected in both soma and dendrites of DARPP32+ cells (Figures 7F–7I). Remarkably, Caspr3-ECD expression increased the number of TH+BSN+ puncta onto GFP+ dendrites of $Nrg3^{f/f}$ mice (Figures 7J–7N). This effect was not observed with Caspr3-$ECD^{\Delta LamG1}$, an ECD mutant that interacts poorly with NRG3 (Figures 5E and S5E–S5G). These data indicate a critical role of the NRG3-Caspr3 interaction in regulating BSN clusters and support the hypothesis. Notice that ECD expression in DAT-$Nrg3^{f/f}$ mice did not further increase the density of TH+BSN+ puncta onto GFP+ dendrites, indicating that the effects of ECD expression and NRG3 mutation were not additive and suggesting that they work via a similar mechanism. Finally, Caspr3 ECD increased the number of axodendritic synapses but had little effect on axospinous synapses, suggesting a potential subcellular regulatory mechanism.

DISCUSSION

This paper provides evidence for in *trans* NRG3-Caspr3 interaction to control DA axonal BSN cluster development. DA axonal

Please cite this article in press as: Cui et al., In *trans* neuregulin3-Caspr3 interaction controls DA axonal bassoon cluster development, Current Biology (2021), https://doi.org/10.1016/j.cub.2021.05.045

CellPress

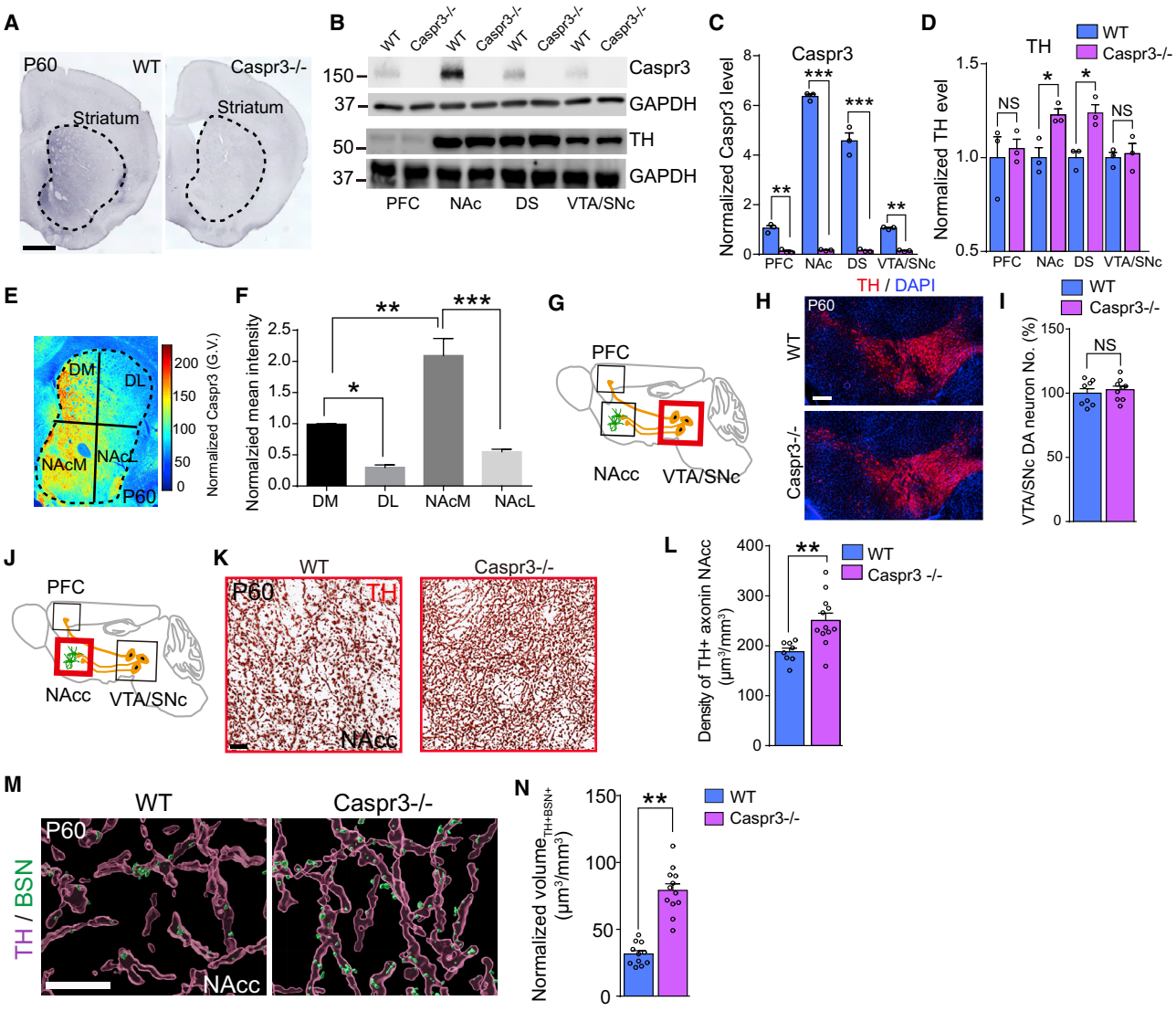

Figure 6. Increased DA axonal BSN clusters in the NAcc of Caspr3$^{-/-}$ mice

(A) Caspr3 is enriched in the mouse striatum. Scale bar, 500 μm.

(B–D) Increased TH in NAc and DS of Caspr3$^{-/-}$ mice.

(B) Representative blots.

(C) Quantification of Caspr3 in (B). ***p < 0.001. Effect of genotype, $F_{(1.20)}$ = 18.27, p = 0.0004. ***p < 0.001, **p < 0.01.

(D) Quantification of TH in (B). Effect of genotype, $F_{(1.16)}$ = 11.31, p = 0.004. Two-way ANOVA followed by Sidak's post hoc. NS, not significant. *p < 0.05.

(E) Heatmap of Caspr3 protein in striatum quantified by the gray value. Scale bar, 200 μm.

(F) Quantification of Caspr3 level in (E). $F_{(3.8)}$ = 32.109. n = 3 slices from 3 mice. One-way ANOVA followed by Sidak's multiple comparison. *p < 0.05, **p < 0.01, ***p < 0.001.

(G and H) No difference in the number of TH+ neurons in the VTA/SNc region between WT and Caspr3$^{-/-}$ mice.

(I) Quantification of (H). p = 0.5444, t = 0.6203. n = 8 for WT and n = 9 for Caspr3$^{-/-}$ mice. Student's t test. Scale bars, mean ± SEM.

(J and K) Increased density of TH+ axons in NAcc of Caspr3$^{-/-}$. Scale bar, 5 μm.

(L) Quantification of (J) and (K). p = 0.004, t = 3.299. n = 8–12 slices from 3 WT and 3 Caspr3$^{-/-}$ mice. **p < 0.01. Student's t test.

(M and N) Increased DA axonal BSN clusters in NAcc of Caspr3$^{-/-}$ mice. Scale bar, 2 μm.

(M) 3D images of DA axonal BSN clusters.

(N) Quantification of (M). **p < 0.01, t = 8.284. n = 12–13 slices from 3 mice for each group. **p < 0.01. Student's t test.

See also Figures S5–S7.

BSN clusters in DAT-*Nrg3*$^{f/f}$ mice were similar to those in control mice at neonatal stages, suggesting that NRG3 may not be necessary for the initial formation of DA synapses. However, more BSN clusters in adult mutant mice suggest increased maintenance and/or reduced elimination. We posit that DA synapse pruning requires the in *trans* NRG3-Caspr3 interaction. First, NRG3 is expressed highly in DA neurons whereas Caspr3 is enriched in striatal MSNs. Second, HEK293 cells expressing

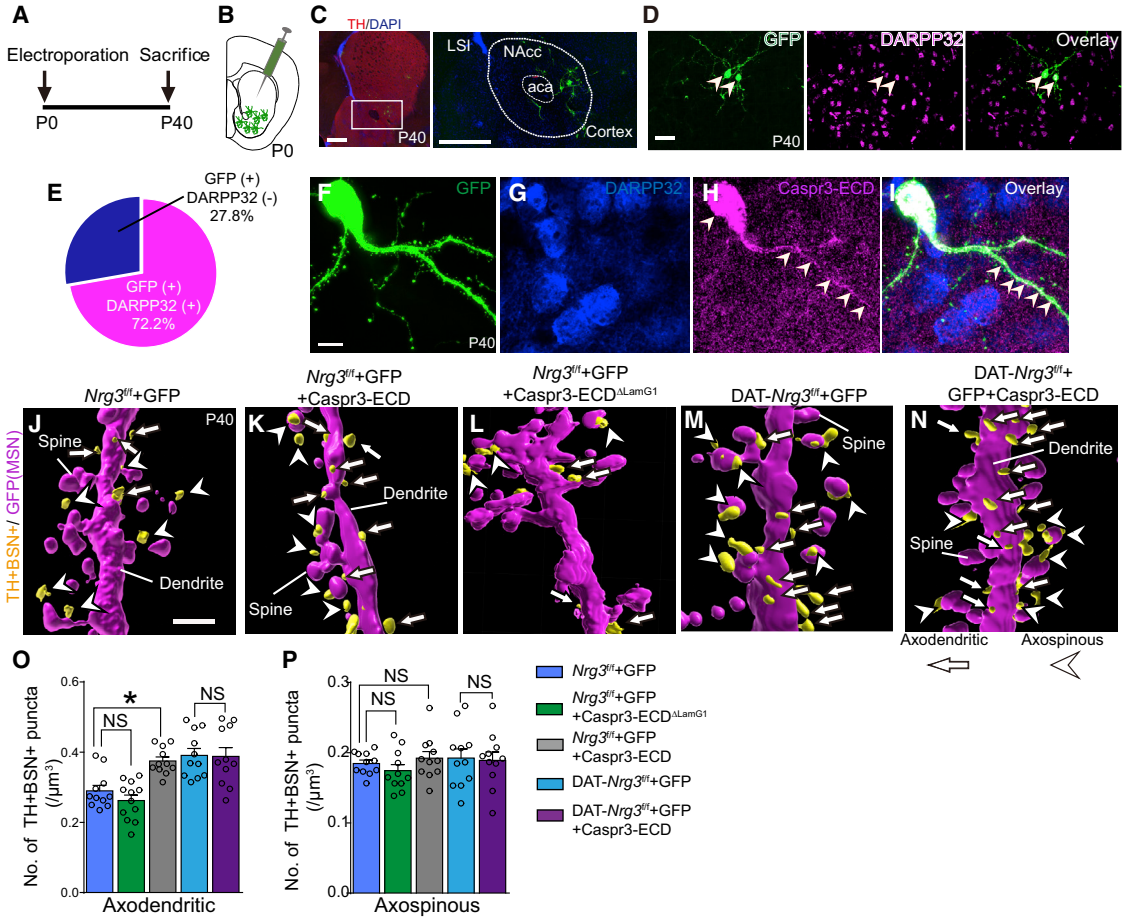

Figure 7. Disruption of NRG3-Caspr3 interaction increased DA axonal BSN clusters on MSNs

(A) Experimental design of postnatal iontoporation in the NAcc.

(B) Schematic diagram showing iontoporation in the ventral striatum.

(C) Representative MSNs were identified by GFP signal after the iontoporation (left). Enlargement (right). Scale bar, 500 μm.

(D) Colocalization of transfected cells with DARPP32. Scale bars, 50 μm.

(E) Quantification of (D). n = 405 cells.

(F–I) Localization of Caspr3-ECDs in an MSN cotransfected with GFP and Caspr3-ECD. Arrowheads indicate the signal of Caspr3 in the MSN. Scale bar, 20 μm.

(J–N) Caspr3-ECD overexpression in MSNs increased DA axonal BSN clusters apposing on MSN dendrites. Scale bar, 3 μm. Arrows, axodendritic synapses; arrowheads, axospinous synapses.

(O) Quantification of axodendritic TH+BSN+ in (J)–(N). *Nrg3*$^{f/f}$+GFP versus *Nrg3*$^{f/f}$+GFP+Caspr3-ECD$^{\Delta LamG1}$, p = 0.805. *Nrg3*$^{f/f}$+GFP versus *Nrg3*$^{f/f}$+GFP+Caspr3-ECD, p < 0.05. DAT-*Nrg3*$^{f/f}$+GFP versus DAT-*Nrg3*$^{f/f}$+GFP+Caspr3-ECD, p = 0.9995. $F_{(3,40)}$ = 6.619.

(P) Quantification of axospinous TH+BSN+ in (J)–(N). Number of TH+BSN+ puncta contacting *Nrg3*$^{f/f}$+GFP versus *Nrg3*$^{f/f}$+GFP+Caspr3-ECD$^{\Delta LamG1}$, p = 0.9475. *Nrg3*$^{f/f}$+GFP versus *Nrg3*$^{f/f}$+GFP+Caspr3-ECD, p = 0.9525. DAT-*Nrg3*$^{f/f}$+GFP versus DAT-*Nrg3*$^{f/f}$+GFP+Caspr3-ECD, p = 0.9958. $F_{(3,40)}$ = 0.1252. One-way ANOVA followed by Tukey's post hoc. Scale bars, mean ± SEM. n = 11–12 cells from 4 mice for each group. NS, not significant.

NRG3 and Caspr3 individually form aggregates that could be blocked by the ECD of Caspr3. Third, more DA axonal BSN clusters and increased DA transmission were observed in mice lacking either NRG3 in DA neurons or Caspr3, providing genetic evidence for the model. Finally, when the NRG3-Caspr3 interaction was blocked *in vivo* by Caspr3 ECD, DA axonal BSN clusters were increased.

During development, the nervous system undergoes fine-tuning when extra neurons die out, axons and dendrites are pruned, and synapses are eliminated.[43] For example, muscle fibers of vertebrates are innervated by multiple motor axons initially, but one fiber receives input from a motor axon in adult animals.[44] In the cerebellum, Purkinje cells (PCs) are innervated by more than one climbing fiber (CF) early on, but by only one eventually.[45] The molecular mechanisms of synapse elimination are not well understood. The maintenance of excitatory synapses in cultured hippocampal neurons requires leucine-rich repeat transmembrane proteins (LRRTMs) and NLGNs, both ligands of NRXNs.[46] Expression of neuroglia (Nrgn), an L1-type CAM, suppresses dendrite pruning, whereas its deletion promotes dendrites elimination.[47] There is a developmental DA neuron death;[48,49] however, the number of DA neurons was not altered by NRG3 or Caspr3 mutation. In the NAcc, the density of DA synapses peaks during the first two postnatal weeks.[19] This is associated with increased NRG3 (Figure 1N); loss of NRG3 increases axonal BSN clusters, suggesting the involvement of NRG3 in DA synapse elimination.

Please cite this article in press as: Cui et al., In *trans* neuregulin3-Caspr3 interaction controls DA axonal bassoon cluster development, Current Biology (2021), https://doi.org/10.1016/j.cub.2021.05.045

NRG3 is a ligand known to bind and activate ErbB4.[37] However, nestin-Cre;*ErbB4*$^{f/f}$ mice were normal in the number of DA neurons and DA axon projections to the basal ganglia.[50] BSN clusters were not changed by ErbB4 mutation. On the contrary, NRG1-ErbB4 signaling was shown to increase DA release; DA levels in the PFC and striatum were reduced in ErbB4 null mice.[38,51] These observations suggest that NRG3 regulates DA synapses in a mechanism independent of ErbB4. Non-based screens for NRG3 binding proteins from a library consisting of many transmembrane molecules implicated in synaptogenesis identified Caspr3 and ErbB4. We provide evidence that NRG3 and Caspr3 are a novel pair of transmembrane proteins for DA synapse development. Caspr3 is located in the dendritic shafts of MSNs (Figure S6F) where 63% of DA synapses onto MSNs are located.[17] Disrupting the NRG3-Caspr3 interaction increased axodendritic DA synapses (Figures 7J–7P). However, the underlying mechanisms of the NRG3-Caspr3 interaction remain unclear. Caspr3 was shown to interact with NLGN2, a protein that has been implicated in *in vitro* DA synapse formation.[24] Whether NLGN2 is regulated by the NRG3-Caspr3 interaction warrants further studies. Many transmembrane proteins, like thrombospondins, neuronal pentraxins, and cerebellins, undergo extracellular shedding to release soluble ECDs.[52] Thus, transmembrane NRG3 or Caspr3 may serve as a receptor for one another's soluble ECD (as a ligand). These hypotheses and how the two proteins assemble pre- and post-synaptic assemblies in corresponding DA axons and MSN dendrites warrant future studies.

Dysregulation of DA transmission has been implicated in neuropsychiatric disorders.[12,13,15] Genetic studies associated SNPs in the NRG3 gene with SZ.[53–55] On the other hand, *de novo* mutations of Caspr3 are identified in patients with autism spectrum disorder. Impaired learning and memory tasks and social behavior were observed in patients with Caspr3 mutation and mutant mice.[56] Here we show that DA neuron-specific NRG3 mutant mice are impaired in CPP, working memory, and locomotor activity. Our study provides molecular insight into pathological mechanisms of relevant neuropsychiatric disorders.

STAR★METHODS

Detailed methods are provided in the online version of this paper and include the following:

- KEY RESOURCES TABLE
- RESOURCE AVAILABILITY
  - Lead contact
  - Materials availability
  - Data and code availability
- EXPERIMENTAL MODEL AND SUBJECT DETAILS
  - Mouse lines
  - Cell lines
- METHOD DETAILS
  - DNA constructs
  - ELISA based ligand-receptor screening
  - Behavioral tests
  - Injections and iontoporation in neonatal mice
  - Cell transfection
  - Tissue collections and biochemical characterization
  - Immunohistochemistry (IHC) and EM
  - MAP and tissue expansion
  - Imaging and data processing
  - *In situ* hybridization
  - Quantitative real-time PCR (qPCR) of mRNAs in tissues and single cells
  - Purification and conjugation of Caspr3-ECDs
  - Cell aggregation assay
  - Slice electrophysiology and Single-unit recordings
  - FSCV
  - DA and 5-HT measurement
- QUANTIFICATION AND STATISTICAL ANALYSIS

SUPPLEMENTAL INFORMATION

Supplemental information can be found online at https://doi.org/10.1016/j.cub.2021.05.045.

ACKNOWLEDGMENTS

We thank Dr. Yasushi Shimoda for providing antibodies and plasmids for Caspr3, Dr. Cary Lai for NRG3 antibodies, Dr. Peng Zhang for comments on the manuscript, and members of the L.M. and W.-C.X. labs for discussions. This study was supported by NSF IOS grants (#1755189 and MCB-1450895 to D.C.), RWJ Foundation grant (#74260 to D.C.), the Fred & Santa Barile Children's Medical Research Trust to D.C., and a grant from the United States NIH (MH083317 to L.M.).

AUTHOR CONTRIBUTIONS

Conceptualization, W.C. and L.M.; Methodology, L.M., W.-C.X., and W.C.; Investigation, W.C., N.G., Z.D., C.S., H.Z., P.C., B.L., H.J., H.W., D.C., and H.R.; Data Analysis, W.C., N.G., Z.D., B.L., and H.Z.; Writing – Original Draft, W.C.; Writing – Review & Editing, L.M., D.C., and W.C.; Funding Acquisition, L.M.; Supervision, L.M. D.C., and W.-C.X.

DECLARATION OF INTERESTS

The authors declare no conflicts of interest.

Received: November 24, 2020
Revised: March 19, 2021
Accepted: May 20, 2021
Published: June 17, 2021

REFERENCES

1. Chechik, G., Meilijson, I., and Ruppin, E. (1999). Neuronal regulation: a mechanism for synaptic pruning during brain maturation. Neural Comput. *11*, 2061–2080.
2. Paolicelli, R.C., Bolasco, G., Pagani, F., Maggi, L., Scianni, M., Panzanelli, P., Giustetto, M., Ferreira, T.A., Guiducci, E., Dumas, L., et al. (2011). Synaptic pruning by microglia is necessary for normal brain development. Science *333*, 1456–1458.
3. Colman, H., Nabekura, J., and Lichtman, J.W. (1997). Alterations in synaptic strength preceding axon withdrawal. Science *275*, 356–361.
4. Matsumoto, M., and Hikosaka, O. (2009). Two types of dopamine neuron distinctly convey positive and negative motivational signals. Nature *459*, 837–841.
5. da Silva, J.A., Tecuapetla, F., Paixão, V., and Costa, R.M. (2018). Dopamine neuron activity before action initiation gates and invigorates future movements. Nature *554*, 244–248.
6. Glimcher, P.W. (2011). Understanding dopamine and reinforcement learning: the dopamine reward prediction error hypothesis. Proc. Natl. Acad. Sci. USA *108* (*Suppl 3*), 15647–15654.

7. Berridge, K.C., and Robinson, T.E. (1998). What is the role of dopamine in reward: hedonic impact, reward learning, or incentive salience? Brain Res. Brain Res. Rev. *28*, 309–369.
8. Wightman, R.M., and Robinson, D.L. (2002). Transient changes in mesolimbic dopamine and their association with 'reward'. J. Neurochem. *82*, 721–735.
9. Robinson, D.L., Heien, M.L., and Wightman, R.M. (2002). Frequency of dopamine concentration transients increases in dorsal and ventral striatum of male rats during introduction of conspecifics. J. Neurosci. *22*, 10477–10486.
10. Daberkow, D.P., Brown, H.D., Bunner, K.D., Kraniotis, S.A., Doellman, M.A., Ragozzino, M.E., Garris, P.A., and Roitman, M.F. (2013). Amphetamine paradoxically augments exocytotic dopamine release and phasic dopamine signals. J. Neurosci. *33*, 452–463.
11. Schultz, W. (1998). Predictive reward signal of dopamine neurons. J. Neurophysiol. *80*, 1–27.
12. Cross, A.J., Crow, T.J., Longden, A., Owen, F., Poulter, M., and Riley, G.J. (1978). Evidence for increased dopamine receptor sensitivity in post mortem brains from patients with schizophrenia [proceedings]. J. Physiol. *280*, 37P.
13. Bymaster, F.P., Katner, J.S., Nelson, D.L., Hemrick-Luecke, S.K., Threlkeld, P.G., Heiligenstein, J.H., Morin, S.M., Gehlert, D.R., and Perry, K.W. (2002). Atomoxetine increases extracellular levels of norepinephrine and dopamine in prefrontal cortex of rat: a potential mechanism for efficacy in attention deficit/hyperactivity disorder. Neuropsychopharmacology *27*, 699–711.
14. Brown, A.S., and Gershon, S. (1993). Dopamine and depression. J. Neural Transm. (Vienna) *91*, 75–109.
15. Mackay, A.V., Iversen, L.L., Rossor, M., Spokes, E., Bird, E., Arregui, A., Creese, I., and Synder, S.H. (1982). Increased brain dopamine and dopamine receptors in schizophrenia. Arch. Gen. Psychiatry *39*, 991–997.
16. Arluison, M., Dietl, M., and Thibault, J. (1984). Ultrastructural morphology of dopaminergic nerve terminals and synapses in the striatum of the rat using tyrosine hydroxylase immunocytochemistry: a topographical study. Brain Res. Bull. *13*, 269–285.
17. Descarries, L., Watkins, K.C., Garcia, S., Bosler, O., and Doucet, G. (1996). Dual character, asynaptic and synaptic, of the dopamine innervation in adult rat neostriatum: a quantitative autoradiographic and immunocytochemical analysis. J. Comp. Neurol. *375*, 167–186.
18. Graybiel, A.M., Pickel, V.M., Joh, T.H., Reis, D.J., and Ragsdale, C.W., Jr. (1981). Direct demonstration of a correspondence between the dopamine islands and acetylcholinesterase patches in the developing striatum. Proc. Natl. Acad. Sci. USA *78*, 5871–5875.
19. Antonopoulos, J., Dori, I., Dinopoulos, A., Chiotelli, M., and Parnavelas, J.G. (2002). Postnatal development of the dopaminergic system of the striatum in the rat. Neuroscience *110*, 245–256.
20. Arbuthnott, G.W., and Wickens, J. (2007). Space, time and dopamine. Trends Neurosci. *30*, 62–69.
21. Pickel, V.M., Beckley, S.C., Joh, T.H., and Reis, D.J. (1981). Ultrastructural immunocytochemical localization of tyrosine hydroxylase in the neostriatum. Brain Res. *225*, 373–385.
22. Pereira, D.B., Schmitz, Y., Mészáros, J., Merchant, P., Hu, G., Li, S., Henke, A., Lizardi-Ortiz, J.E., Karpowicz, R.J., Jr., Morgenstern, T.J., et al. (2016). Fluorescent false neurotransmitter reveals functionally silent dopamine vesicle clusters in the striatum. Nat. Neurosci. *19*, 578–586.
23. Dalva, M.B., McClelland, A.C., and Kayser, M.S. (2007). Cell adhesion molecules: signalling functions at the synapse. Nat. Rev. Neurosci. *8*, 206–220.
24. Uchigashima, M., Ohtsuka, T., Kobayashi, K., and Watanabe, M. (2016). Dopamine synapse is a neuroligin-2-mediated contact between dopaminergic presynaptic and GABAergic postsynaptic structures. Proc. Natl. Acad. Sci. USA *113*, 4206–4211.
25. Matsuda, W., Furuta, T., Nakamura, K.C., Hioki, H., Fujiyama, F., Arai, R., and Kaneko, T. (2009). Single nigrostriatal dopaminergic neurons form widely spread and highly dense axonal arborizations in the neostriatum. J. Neurosci. *29*, 444–453.
26. Ku, T., Swaney, J., Park, J.Y., Albanese, A., Murray, E., Cho, J.H., Park, Y.G., Mangena, V., Chen, J., and Chung, K. (2016). Multiplexed and scalable super-resolution imaging of three-dimensional protein localization in size-adjustable tissues. Nat. Biotechnol. *34*, 973–981.
27. Mei, L., and Nave, K.A. (2014). Neuregulin-ERBB signaling in the nervous system and neuropsychiatric diseases. Neuron *83*, 27–49.
28. Wang, Y.N., Figueiredo, D., Sun, X.D., Dong, Z.Q., Chen, W.B., Cui, W.P., Liu, F., Wang, H.S., Li, H.W., Robinson, H., et al. (2018). Controlling of glutamate release by neuregulin3 via inhibiting the assembly of the SNARE complex. Proc. Natl. Acad. Sci. USA *115*, 2508–2513.
29. Liu, C., Kershberg, L., Wang, J., Schneeberger, S., and Kaeser, P.S. (2018). Dopamine secretion is mediated by sparse active zone-like release sites. Cell *172*, 706–718.e15.
30. Sharpe, M.J., Chang, C.Y., Liu, M.A., Batchelor, H.M., Mueller, L.E., Jones, J.L., Niv, Y., and Schoenbaum, G. (2017). Dopamine transients are sufficient and necessary for acquisition of model-based associations. Nat. Neurosci. *20*, 735–742.
31. Schelp, S.A., Brodnik, Z.D., Rakowski, D.R., Pultorak, K.J., Sambells, A.T., España, R.A., and Oleson, E.B. (2018). Diazepam concurrently increases the frequency and decreases the amplitude of transient dopamine release events in the nucleus accumbens. J. Pharmacol. Exp. Ther. *364*, 145–155.
32. Pultorak, K.J., Schelp, S.A., Isaacs, D.P., Krzystyniak, G., and Oleson, E.B. (2018). A transient dopamine signal represents avoidance value and causally influences the demand to avoid. eNeuro *5*, ENEURO.0058-18.2018.
33. Addy, N.A., Daberkow, D.P., Ford, J.N., Garris, P.A., and Wightman, R.M. (2010). Sensitization of rapid dopamine signaling in the nucleus accumbens core and shell after repeated cocaine in rats. J. Neurophysiol. *104*, 922–931.
34. Exley, R., Clements, M.A., Hartung, H., McIntosh, J.M., and Cragg, S.J. (2008). Alpha6-containing nicotinic acetylcholine receptors dominate the nicotine control of dopamine neurotransmission in nucleus accumbens. Neuropsychopharmacology *33*, 2158–2166.
35. Yorgason, J.T., Zeppenfeld, D.M., and Williams, J.T. (2017). Cholinergic interneurons underlie spontaneous dopamine release in nucleus accumbens. J. Neurosci. *37*, 2086–2096.
36. Liu, C., Goel, P., and Kaeser, P.S. (2021). Spatial and temporal scales of dopamine transmission. Nat. Rev. Neurosci. *22*, 345–358.
37. Zhang, D., Sliwkowski, M.X., Mark, M., Frantz, G., Akita, R., Sun, Y., Hillan, K., Crowley, C., Brush, J., and Godowski, P.J. (1997). Neuregulin-3 (NRG3): a novel neural tissue-enriched protein that binds and activates ErbB4. Proc. Natl. Acad. Sci. USA *94*, 9562–9567.
38. Skirzewski, M., Cronin, M.E., Murphy, R., Fobbs, W., Kravitz, A.V., and Buonanno, A. (2020). ErbB4 null mice display altered mesocorticolimbic and nigrostriatal dopamine levels as well as deficits in cognitive and motivational behaviors. eNeuro *7*, ENEURO.0395-19.2020.
39. Ozgul, S., von Daake, S., Kakehi, S., Sereni, D., Denissova, N., Hanlon, C., Huang, Y.J., Everett, J.K., Yin, C., Montelione, G.T., and Comoletti, D. (2019). An ELISA-based screening platform for ligand-receptor discovery. Methods Enzymol. *615*, 453–475.
40. Ranaivoson, F.M., Turk, L.S., Ozgul, S., Kakehi, S., von Daake, S., Lopez, N., Trobiani, L., De Jaco, A., Denissova, N., Demeler, B., et al. (2019). A proteomic screen of neuronal cell-surface molecules reveals IgLONs as structurally conserved interaction modules at the synapse. Structure *27*, 893–906.e9.
41. Spiegel, I., Salomon, D., Erne, B., Schaeren-Wiemers, N., and Peles, E. (2002). Caspr3 and caspr4, two novel members of the caspr family are expressed in the nervous system and interact with PDZ domains. Mol. Cell. Neurosci. *20*, 283–297.
42. De la Rossa, A., and Jabaudon, D. (2015). In vivo rapid gene delivery into postmitotic neocortical neurons using iontoporation. Nat. Protoc. *10*, 25–32.
43. McAllister, A.K. (2007). Dynamic aspects of CNS synapse formation. Annu. Rev. Neurosci. *30*, 425–450.
44. Sanes, J.R., and Lichtman, J.W. (1999). Development of the vertebrate neuromuscular junction. Annu. Rev. Neurosci. *22*, 389–442.

45. Crepel, F., Mariani, J., and Delhaye-Bouchaud, N. (1976). Evidence for a multiple innervation of Purkinje cells by climbing fibers in the immature rat cerebellum. J. Neurobiol. *7*, 567–578.

46. Ko, J., Soler-Llavina, G.J., Fuccillo, M.V., Malenka, R.C., and Südhof, T.C. (2011). Neuroligins/LRRTMs prevent activity- and Ca2+/calmodulin-dependent synapse elimination in cultured neurons. J. Cell Biol. *194*, 323–334.

47. Zhang, H., Wang, Y., Wong, J.J., Lim, K.L., Liou, Y.C., Wang, H., and Yu, F. (2014). Endocytic pathways downregulate the L1-type cell adhesion molecule neuroglian to promote dendrite pruning in Drosophila. Dev. Cell *30*, 463–478.

48. Ries, V., Cheng, H.C., Baohan, A., Kareva, T., Oo, T.F., Rzhetskaya, M., Bland, R.J., During, M.J., Kholodilov, N., and Burke, R.E. (2009). Regulation of the postnatal development of dopamine neurons of the substantia nigra in vivo by Akt/protein kinase B. J. Neurochem. *110*, 23–33.

49. Burke, R.E. (2004). Ontogenic cell death in the nigrostriatal system. Cell Tissue Res. *318*, 63–72.

50. Thuret, S., Alavian, K.N., Gassmann, M., Lloyd, C.K., Smits, S.M., Smidt, M.P., Klein, R., Dyck, R.H., and Simon, H.H. (2004). The neuregulin receptor, ErbB4, is not required for normal development and adult maintenance of the substantia nigra pars compacta. J. Neurochem. *91*, 1302–1311.

51. Yurek, D.M., Zhang, L., Fletcher-Turner, A., and Seroogy, K.B. (2004). Supranigral injection of neuregulin1-beta induces striatal dopamine overflow. Brain Res. *1028*, 116–119.

52. Ferrer-Ferrer, M., and Dityatev, A. (2018). Shaping synapses by the neural extracellular matrix. Front. Neuroanat. *12*, 40.

53. Fallin, M.D., Lasseter, V.K., Wolyniec, P.S., McGrath, J.A., Nestadt, G., Valle, D., Liang, K.Y., and Pulver, A.E. (2003). Genomewide linkage scan for schizophrenia susceptibility loci among Ashkenazi Jewish families shows evidence of linkage on chromosome 10q22. Am. J. Hum. Genet. *73*, 601–611.

54. Morar, B., Dragović, M., Waters, F.A., Chandler, D., Kalaydjieva, L., and Jablensky, A. (2011). Neuregulin 3 (NRG3) as a susceptibility gene in a schizophrenia subtype with florid delusions and relatively spared cognition. Mol. Psychiatry *16*, 860–866.

55. Kao, W.T., Wang, Y., Kleinman, J.E., Lipska, B.K., Hyde, T.M., Weinberger, D.R., and Law, A.J. (2010). Common genetic variation in Neuregulin 3 (NRG3) influences risk for schizophrenia and impacts NRG3 expression in human brain. Proc. Natl. Acad. Sci. USA *107*, 15619–15624.

56. Tong, D.L., Chen, R.G., Lu, Y.L., Li, W.K., Zhang, Y.F., Lin, J.K., He, L.J., Dang, T., Shan, S.F., Xu, X.H., et al. (2019). The critical role of ASD-related gene CNTNAP3 in regulating synaptic development and social behavior in mice. Neurobiol. Dis. *130*, 104486.

57. Tidcombe, H., Jackson-Fisher, A., Mathers, K., Stern, D.F., Gassmann, M., and Golding, J.P. (2003). Neural and mammary gland defects in ErbB4 knockout mice genetically rescued from embryonic lethality. Proc. Natl. Acad. Sci. USA *100*, 8281–8286.

58. Hirata, H., Umemori, J., Yoshioka, H., Koide, T., Watanabe, K., and Shimoda, Y. (2016). Cell adhesion molecule contactin-associated protein 3 is expressed in the mouse basal ganglia during early postnatal stages. J. Neurosci. Res. *94*, 74–89.

59. Dong, Z., Chen, W., Chen, C., Wang, H., Cui, W., Tan, Z., Robinson, H., Gao, N., Luo, B., Zhang, L., et al. (2020). CUL3 deficiency causes social deficits and anxiety-like behaviors by impairing excitation-inhibition balance through the promotion of cap-dependent translation. Neuron *105*, 475–490.e6.

60. Nygaard, K.R., Maloney, S.E., and Dougherty, J.D. (2019). Erroneous inference based on a lack of preference within one group: autism, mice, and the social approach task. Autism Res. *12*, 1171–1183.

61. Itzhak, Y., and Martin, J.L. (2002). Cocaine-induced conditioned place preference in mice: induction, extinction and reinstatement by related psychostimulants. Neuropsychopharmacology *26*, 130–134.

62. Cui, W., Aida, T., Ito, H., Kobayashi, K., Wada, Y., Kato, S., Nakano, T., Zhu, M., Isa, K., Kobayashi, K., et al. (2020). Dopaminergic signaling in the nucleus accumbens modulates stress-coping strategies during inescapable stress. J. Neurosci. *40*, 7241–7254.

63. Cui, W., Mizukami, H., Yanagisawa, M., Aida, T., Nomura, M., Isomura, Y., Takayanagi, R., Ozawa, K., Tanaka, K., and Aizawa, H. (2014). Glial dysfunction in the mouse habenula causes depressive-like behaviors and sleep disturbance. J. Neurosci. *34*, 16273–16285.

64. Huff, J., Bergter, A., Birkenbeil, J., Kleppe, I., and Engelmann, R. (2017). The new 2D superresolution mode for ZEISS Airyscan. Nat. Methods *14*, 1223.

65. Aida, T., Yoshida, J., Nomura, M., Tanimura, A., Iino, Y., Soma, M., Bai, N., Ito, Y., Cui, W., Aizawa, H., et al. (2015). Astroglial glutamate transporter deficiency increases synaptic excitability and leads to pathological repetitive behaviors in mice. Neuropsychopharmacology *40*, 1569–1579.

66. Wu, H., Barik, A., Lu, Y., Shen, C., Bowman, A., Li, L., Sathyamurthy, A., Lin, T.W., Xiong, W.C., and Mei, L. (2015). Slit2 as a β-catenin/Ctnnb1-dependent retrograde signal for presynaptic differentiation. eLife *4*, e07266.

67. Biederer, T., Sara, Y., Mozhayeva, M., Atasoy, D., Liu, X., Kavalali, E.T., and Südhof, T.C. (2002). SynCAM, a synaptic adhesion molecule that drives synapse assembly. Science *297*, 1525–1531.

68. Liu, X., Chen, Y., Tong, J., Reynolds, A.M., Proudfoot, S.C., Qi, J., Penzes, P., Lu, Y., and Liu, Q.S. (2016). Epac signaling is required for cocaine-induced change in AMPA receptor subunit composition in the ventral tegmental area. J. Neurosci. *36*, 4802–4815.

69. Grace, A.A., and Bunney, B.S. (1983). Intracellular and extracellular electrophysiology of nigral dopaminergic neurons–1. Identification and characterization. Neuroscience *10*, 301–315.

70. Hazan, L., Zugaro, M., and Buzsáki, G. (2006). Klusters, NeuroScope, NDManager: a free software suite for neurophysiological data processing and visualization. J. Neurosci. Methods *155*, 207–216.

71. Grace, A.A., and Bunney, B.S. (1984). The control of firing pattern in nigral dopamine neurons: single spike firing. J. Neurosci. *4*, 2866–2876.

72. Soden, M.E., Jones, G.L., Sanford, C.A., Chung, A.S., Güler, A.D., Chavkin, C., Luján, R., and Zweifel, L.S. (2013). Disruption of dopamine neuron activity pattern regulation through selective expression of a human KCNN3 mutation. Neuron *80*, 997–1009.

73. Clark, J.J., Sandberg, S.G., Wanat, M.J., Gan, J.O., Horne, E.A., Hart, A.S., Akers, C.A., Parker, J.G., Willuhn, I., Martinez, V., et al. (2010). Chronic microsensors for longitudinal, subsecond dopamine detection in behaving animals. Nat. Methods *7*, 126–129.

74. Wightman, R.M., Heien, M.L., Wassum, K.M., Sombers, L.A., Aragona, B.J., Khan, A.S., Ariansen, J.L., Cheer, J.F., Phillips, P.E., and Carelli, R.M. (2007). Dopamine release is heterogeneous within microenvironments of the rat nucleus accumbens. Eur. J. Neurosci. *26*, 2046–2054.

75. Bucher, E.S., Brooks, K., Verber, M.D., Keithley, R.B., Owesson-White, C., Carroll, S., Takmakov, P., McKinney, C.J., and Wightman, R.M. (2013). Flexible software platform for fast-scan cyclic voltammetry data acquisition and analysis. Anal. Chem. *85*, 10344–10353.

76. Vogeser, M., and Parhofer, K.G. (2007). Liquid chromatography tandem-mass spectrometry (LC-MS/MS)–technique and applications in endocrinology. Exp. Clin. Endocrinol. Diabetes *115*, 559–570.

77. Faul, F., Erdfelder, E., Lang, A.G., and Buchner, A. (2007). G*Power 3: a flexible statistical power analysis program for the social, behavioral, and biomedical sciences. Behav. Res. Methods *39*, 175–191.

Please cite this article in press as: Cui et al., In *trans* neuregulin3-Caspr3 interaction controls DA axonal bassoon cluster development, Current Biology (2021), https://doi.org/10.1016/j.cub.2021.05.045

STAR★METHODS

KEY RESOURCES TABLE

REAGENT or RESOURCE	SOURCE	IDENTIFIER
Antibodies		
Polyclonal Rabbit anti-NRG3 (1:500 for immunohistochemistry, 1:1000 for western and Co-IP)	a gift from Dr. Carry Lai	Cat#: 6144; RRID: AB_2832214
Polyclonal rat anti-Caspr3 (1:500 for immunohistochemistry, 1:1000 for western and Co-IP)	a gift from Dr. Yasushi Shimoda	Cat#: 1G6 and 3A2; RRID: AB_2832215
Polyclonal rabbit anti-tdTomato (1:500 for immunohistochemistry, 1:1000 for western and Co-IP)	abcam	Cat#: ab62341; RRID: AB_945213
Polyclonal rabbit anti-GAPDH (1:2000 for western and Co-IP)	abcam	Cat#: ab9485; RRID: AB_307275
Monoclonal mouse anti-Tyrosine hydroxylase (1:500 for immunohistochemistry, 1:2000 for western and Co-IP)	Santa Cruz	Cat#: sc-25269; RRID: AB_628422
Polyclonal rabbit anti-GFP (1:2000 for western and Co-IP)	Thermo Fisher Scientific	Cat#: A-11122; RRID: AB_221569
Monoclonal mouse anti-NL2 (1:1000 for western and Co-IP)	Synaptic Systems	Cat#: 129511(5E6); RRID: AB_2619813
Monoclonal mouse anti-Myc (1:1000 for western and Co-IP)	Cell Signaling Technology	Cat#: 2276 (9B11); RRID: AB_331783
Polyclonal rabbit anti-Flag (1:1000 for western and Co-IP)	Sigma-Aldrich	Cat#: F7425; RRID: AB_439687
Monoclonal mouse anti-β-actin (1:2000 for western and Co-IP)	Cell Signaling Technology	Cat#:4967; RRID: AB_330288
Monoclonal mouse anti-bassoon (1:500 for immunohistochemistry)	Enzo life sciences	Cat# ADI-VAM-PS003-F; RRID: AB_11181058
Polyclonal rabbit anti-Vesicular Monoamine Transporter2 (VMAT2) (1:500 for immunohistochemistry)	ImmunoStar	Cat#20042; RRID: AB_10891018
Monoclonal mouse anti-Tau (1:500 for immunohistochemistry)	Millipore	Cat#: MAB3420; RRID: AB_94855
Goat anti-rabbit IgG HRP-conjugated (1:5000 for western and Co-IP)	abcam	Cat#: ab6721; RRID: AB_955447
Goat anti-rat IgG HRP-conjugated (1:5000 for western and Co-IP)	abcam	Cat#: ab97057; RRID: AB_10680316
Goat anti-mouse IgG HRP-conjugated (1:5000 for western and Co-IP)	abcam	Cat#: ab6728; RRID: AB_955440
Monoclonal mouse anti-DARPP32 (1:500 for immunohistochemistry)	Santa Cruz	Cat#: sc-271111; RRID: AB_10610055
Bacterial and virus strains		
AAV2/5-CMV-GFP	UNC	https://infoporte.unc.edu/cores/items.php?iid=361&cid=43
AAV2/5-CMV-NRG3-GFP	Custom made	N/A
Chemicals, peptides, and recombinant proteins		
Carbon fiber filament	Goodfellow	Cat#: C005722/5
Raclopride	Sigma	Cat#: R121-25MG
Dopamine hydrochloride	Sigma	Cat#: H8502
Serotonin hydrochloride	Sigma	Cat#: H9523

(*Continued on next page*)

Please cite this article in press as: Cui et al., In *trans* neuregulin3-Caspr3 interaction controls DA axonal bassoon cluster development, Current Biology (2021), https://doi.org/10.1016/j.cub.2021.05.045

Continued

REAGENT or RESOURCE	SOURCE	IDENTIFIER
30% Acrylamide/Bis Solution, 19:1	Bio-Rad	Cat#: 1610154
Acetamide	Sigma	Cat#: 00160
Dihydro-b-erythroidine (DHβE)	TOCRIS	Cat. #: 2349
Experimental models: Cell lines		
HEK293T cell	ATCC	ATCC Cat# CRL-3216; RRID: CVCL_0063
Experimental models: Organisms/Strains		
Mouse: B6.SJL-Slc6a3$^{tm1.1(cre)Bkmn}$/J	Jackson laboratory	RRID: IMSR_JAX: 006660
Mouse: B6;129S-Gt(ROSA) 26Sor$^{tm34.1(CAGSyp/tdTomato)Hze}$/J	Jackson laboratory	RRID: IMSR_JAX: 012570
Erbb4−/−; Tg(MHC-ErbB4	MGI	RRID: MGI:5318192
C57BL/6NJ-Cntnap3em1(IMPC)J/Mmjax	Jackson laboratory	RRID: MMRRC_043708-JAX
Oligonucleotides		
See Table S4	N/A	N/A
Recombinant DNA		
pNICE-LAP-neurexin-1beta	Addgene	Addgene plasmid # 42575; RRID: Addgene_42575
pNICE-NL2A	Addgene	Addgene plasmid # 15259; RRID: Addgene_15259
pCDNA3.1-Flag-Caspr3$^{\Delta LamG1}$	Custom made	Available upon request
pCDNA3.1-Flag-Caspr3$^{\Delta LamG2}$	Custom made	Available upon request
pCDNA3.1-Flag-Caspr3$^{\Delta LamG3}$	Custom made	Available upon request
pCDNA3.1-Flag-Caspr3$^{\Delta LamG4}$	Custom made	Available upon request
Software and algorithms		
MATLAB	MathWorks	RRID: SCR_001622
HDCV	The University of North Carolina at Chapel Hill	http://www.chem.unc.edu/facilities/electronics_software.htm
ImageJ Fiji	NIH	RRID: SCR_002285
Adobe Photoshop CS5	Adobe Systems, San Jose, CA	RRID: SCR_014199
Noldus EthoVision	Ethovision Software	RRID: SCR_000441
Imaris 9.50	Bitplane	RRID: SCR_007370
MATLAB code for data analysis	This paper	https://github.com/WPCCASE/NRG3.git

RESOURCE AVAILABILITY

Lead contact

Further information and requests for resources and reagents should be directed to and will be fulfilled by the Lead Contact, Lin Mei (lin.mei@case.edu).

Materials availability

All unique/stable reagents generated in this study are available from the Lead Contact, with a completed Materials Transfer Agreement.

Data and code availability

The MATLAB code generated during this study is available at [Github] [https://github.com/WPCCASE/NRG3.git].

EXPERIMENTAL MODEL AND SUBJECT DETAILS

Mouse lines

For experiments of histology, behavior, electrophysiology, investigators were blind to genotypes or treatments. Procedures with animals were approved by the Institutional Animal Care and Use Committee of Case Western Reserve University. Mice were housed on a 12-h light/dark (light on from 6:00 AM-6:00 PM) cycle schedule and *ad libitum* water and food. Both male and female mice were used for histology, biochemical, electrochemical, and electrophysiology recordings. 8- to 12-week-old male mice were used in behavioral experiments. Generation of *Nrg3*$^{f/f}$ mice was described in the previous study.[28] Genotyping of *Nrg3*$^{f/f}$ mice was performed

Please cite this article in press as: Cui et al., In *trans* neuregulin3-Caspr3 interaction controls DA axonal bassoon cluster development, Current Biology (2021), https://doi.org/10.1016/j.cub.2021.05.045

using a pair of primers (forward, 5′-TGGAC TTCAG CGAGA GACAC-3′, reverse 5′-CTTCT CCTTC CAGCT CTAG-3′). The amplicon with 230 bp indicating wild-type *Nrg3* allele, and 345 bp for the floxed *Nrg*3 allele. Caspr3−/− mice were purchased from Jackson (Stock No.: 43708-JAX) and genotyped with a forward primer 5′-CTGGA GTGGA TGTAG CAA-3′, and a reverse 5′-AGGAG TTAGT AGAAG TCTCA-3′. The PCR products for Caspr3−/− mice were 535 bp for WT mice, and 257 bp for Caspr3−/− mice. *DAT::Cre* mice were obtained from Jackson Laboratory (Stock No.: 006660). Mice carrying *DAT::Cre* were identified using the following primer sets (forward, TGGCT GTTGG TGTAA AGTGG, reverse_WT GGACA GGGAC ATGGT TGACT, reverse_mutant CCAAA AGACG GCAAT ATGGT). *Ai14* mice were purchased from Jackson (Stock No.: 012570). ErbB4 −/− mice were generated by transgenic expression of human ErbB4 (HER4) under a cardiac-specific myosin promoter in ErbB4 knockout mice to rescue midembryonic lethality as reported previously.[57]

Cell lines

HEK293 cells were cultured in DMEM (10013CV, Corning, NY, USA) supplemented with 10% FBS (100–106, Gemini Bio Products, CA, USA) and 1% penicillin/streptomycin (15140122, Thermo Fisher Scientific, MA).

METHOD DETAILS

DNA constructs

Expression vectors were generated according to the previous publication.[28] The full-length cDNA of *Nrg3* was generated by PCR and subcloned into p3 × Flag-CMV and fused with GFP. Expression vectors of pCDNA3.1-Caspr3-ECD-Fc and pCDNA3.1-Flag-Caspr3 were kindly provided by Dr. Yasushi Shimoda.[58] pNICE-LAP-neurexin-1beta (#42575, Addgene, MA, USA) and pNICE-NLGN2A (#15259, Addgene, MA) were purchased from Addgene. Deletion mutants of Caspr3 were generated in pCDNA3.1-Flag-Caspr3 using the Q5 Site-Directed Mutagenesis Kit (New England Biolabs, MA); the primers used were: LamG1 bp 619-1035 (Val207 - Val345) (F: 5′- CCAAG TAGTT TAAGG GAAGT AGTGG ATCCT ATTGCA −3′ and R: 5′- TGCAA TAGGA TCCAC TACTT CCCTT AAACT ACTTGG-3′); LamG2, 1180 - 1182 bp (Asp394 - Lys525) (F: 5′- CCAAG TAGTT TAAGG GAAGT AGTGG ATCCT ATTGCA −3′ and R: 5-TGCAA TAGGA TCCAC TACTT CCCTT AAACT ACTTGG-3′); LamG3, 2243-2826 bp (Leu815 - Met942) (F: 5′- CCAAC CTTCC GTGGA GAGGC ACTAG ACCTG GAGGAA-3′ and R: 5′- TTCCT CCAGG TCTAG TGCCT CTCCA CGGAA GGTTGG-3′; LamG4, 3118-3534 bp (Ser1040 - Glu1178) (F: 5′- CATGG GGATG TCATA CTGGT CCCAC TGAAG GCTGCA-3′ and R: 5′- TGCAG CCTTC AGTGG GACCA GTATG ACATC CCCATG-3′).

ELISA based ligand-receptor screening

ELISA-based screening for the binding partner of NRG3 was performed as reported before.[39] Briefly, NRG3-ECD was subcloned into pCMV6-XL4 and fused with human alkaline phosphatase (AP). NRG3 ECD-AP was used as a bait for binding partners. ECD of prey proteins was fused with fragment crystallizable region (Fc) in pCMV6-XL4, including 382 cell adhesion molecules and receptors that were implicated in neural development (Table S2). NRG3 ECD-AP was collected from the transfected HEK293F culture medium and immobilized to 384-well microtiter plates via a capture antibody (anti-AP antibody). After incubating with 5% dry nonfat milk to reduce nonspecific binding, the plates were incubated with media containing individual prey proteins' ECD. After washing, bound prey ECD-Fc was detected by ELISA with horseradish peroxidase (HRP)-conjugated anti-Fc antibody and 1-Step Ultra TMB-ELISA substrate (34028, Thermo Fisher Scientific, CA). Interaction of Neuroligin1 (NLGN1) and Neurexin1 β (NRXN 1β) was used as a positive control to gauge the sensitivity of the assay, and negative control was prepared by omitting the anti-AP antibody in the well.

Behavioral tests

Before behavioral tests, male mice were submitted to habituation to the test room for at least 1 h.[28] Mice were subjected to o*pen-field test in an* arena (50 × 50 × 20 cm) under the illumination 500 lx and were monitored for 30 min for locomotor activity by using a tracking software system (EthoVision, Noldus, VA, USA). Y-maze was performed by placing mice at the center of Y-maze with three arms (designate as arm A, B, or C). Each arm has the same dimension (35 × 8 × 15 cm) at a 120° angle from each other. Mice were allowed to explore each arm freely for 8 min. The total number and sequence of arm entries were recorded. Spontaneous alternations were determined by entry sequences such as ABC or BCA. First and last arm entries were not included in the total number of entries.

Social interaction test was conducted in a black plexiglass box that consisted of three interconnected chambers (30 × 30 × 20 cm) as previously described.[59] Mice were allowed to explore the three chambers for 10 min; mice showing a preference for any of the three chambers were excluded from the test. To test social preference, the test mouse was placed in the center chamber with both gates to the side chambers closed. A stranger wild-type mouse (S1) was placed in a mesh container in a side chamber while the other chamber had a mesh container with a novel object (O). After opening both gates, the test mouse was monitored for the distance to the S1 and O cages for 10 min. To test social novelty, the test mouse was placed in the center chamber with both gates closed; the S1 mouse was placed in the O cage and a second stranger wild-type mouse (S2) was placed in the previous S1 cage. The test mouse was allowed for free exploration and monitored for the distance to either cage for 10 min. The time when the mouse was within 8 cm interaction zone (sniffing time) was recorded and analyzed using a tracking software (EthoVision, Noldus), as previously described,[59] to directly compare between different groups as well as within groups. Social preference index and social novelty index were calculated as described.[60]

Please cite this article in press as: Cui et al., In *trans* neuregulin3-Caspr3 interaction controls DA axonal bassoon cluster development, Current Biology (2021), https://doi.org/10.1016/j.cub.2021.05.045

Cocaine-induced conditioned place preference (CPP) was performed as previously described with slight modification.[61] Plexiglass box with two separated chambers (25 × 15 × 15 cm), each with distinct texture of flooring (corncob or cellulose) and wall (black or white). On Day 1, mice were allowed to explore the chambers for 20 min freely for habituation. On Day 2, mice were monitored for time spent in the two chambers within 20 min, and those with a preference for either chamber were excluded for further study. On Day 3, mice without chamber preference on Day 2 were injected with cocaine (10 mg/kg, i.p.) and placed in one chamber with the door closed for 30 min. On Day 4, they were injected with saline and placed in the other chamber with the door closed for 30 min. These procedures were repeated for 3 more sessions. On Day 11, mice were injected with single saline, placed in the saline chamber, and monitored for the time spent in each chamber for 20 min.

Injections and iontoporation in neonatal mice

The production and purification of AAV vector were done as described previously.[62] HEK293 cells were co-transfected with pAAV vector plasmid harboring a gene of interest, pAAV-RC2, and pHelper. The viral lysate was purified with cesium chloride ultracentrifugation. The titer of the viral stock was determined against plasmid standards by real-time PCR. Stereotaxic injection in neonatal mice was performed based on previous report with slight modification.[42] C57BL/6J male mice at P0 were anesthetized by isoflurane (2.5% isoflurane in a 30%:70% O_2: N_2 gas mixture). To target the NAc (2.8 mm anterior and 1.0 mm lateral to the vascular lambda) and VTA (0.5 mm anterior and 0.1 mm lateral to the vascular lambda) using a 33-gauge needle. GFP or GFP+Caspr3-ECD or GFP+Caspr3-ECDΔLamG1 (1:2) plasmids were mixed with TCHD. Glass capillary containing the plasmids or viral solution was lowered to a depth of 3.2 mm from the skin surface and 0.2 μl of AAV solution (2.3-3.1 × 10^{10} genome copies/mL) or plasmids mixture (2 μg/μl mixed with TCHD) were injected into the striatum or VTA at a speed of 0.02 μl/min. Five minutes after the injection, the glass capillary was withdrawn gently from the brain. 10 pulses at 99 V was applied twice with an interval of 10 s in iontoporation.

Cell transfection

Transient transfection was performed using polyethylenimine (15140122, Sigma-Aldrich, MO) as described previously with modifications.[28] Briefly, cells were cultured in a 100-mm dish (at ~70% cell confluence) and transfected by 5 μg of plasmid DNA with 10 μL of 0.5% polyethylenimine (wt/vol.) mixed in 1 mL Opti-MEM (31985062, Thermo Fisher Scientific, MA). 48 h after transfection, cells were lysed and subjected to biochemical characterization.

Tissue collections and biochemical characterization

Tissues of different brain regions were collected by coronal sections with the following coordinates: PFC sections (500 μm, around 2.0 mm to 1.50 mm anterior to bregma), striatum including DS (1st part, 600 μm, 1.30 mm to 0.70 mm anterior to bregma, 2nd part, 700 μm around 0.80 mm to 0.10 mm anterior to bregma), NAc (600 μm, around 1.30 mm to 0.70 mm anterior to bregma) and VTA/SNc (700 μm, −3.20 mm to 3.90 mm posterior to bregma). Sections were prepared with a vibrotome (VT1000S, Leica Biosytems, IL, USA) in oxygenized PBS buffer on ice. Tissues of interested regions were dissected under a fluorescent stereo microscope (MVX10, Olympus, Japan). Tissues and cells were homogenized in modified RIPA buffer [150 mM NaCl, 50 mM Tris-HCl, pH 7.4, 2 mM EDTA, 0.1% SDS, 1 mM phenylmethylsulfonyl fluoride (PMSF), 0.5% sodium deoxycholate, 5 mM NaF, 2 mM Na_3VO_4, and protease inhibitors (4693132001, Roche, Switzerland). Samples were centrifuged at 12,000 × g for 10 min at 4°C to remove debris. Protein concentration was determined by Pierce BCA Protein Assay Kit (23225, Thermo Fisher Scientific, MA). Samples (50 μg of protein) were resolved by SDS-PAGE, transferred to nitrocellulose membranes, and probed with primary and secondary antibodies (STAR Methods).

HEK293T cells were individually transfected with plasmids expressing NRG3-ECD-AP and Caspr3-ECD-Fc, culture medium from both groups was mixed to form NRG3-Caspr3 complex. Anti-Flag antibody or control antibody (IgG) was used to precipitate the NRG3 complex. Caspr3-ECD were blotted using an anti-Caspr3 antibody, NRG3-ECD were probed with an anti-Flag antibody. For co-immunoprecipitation assays (Co-IP), cell lysates or homogenates were incubated with protein A/G agarose beads (sc-2003, Santa Cruz, CA) for 1 h at 4°C. Pre-cleared samples were incubated with rat anti-Caspr3 (1:300, 1G6, a gift from Dr. Yasushi Shimoda), followed by protein A/G agarose beads for 4 h at 4°C (20423, Thermo Fisher Scientific, MA). For Flag-tagged proteins, samples were incubated with anti-Flag M2 affinity gel (1:200, A2220, Sigma-Aldrich, MO) for 4 h at 4°C. Beads were washed three times with lysis buffer. Precipitated proteins and 5 −10% total lysates were subjected to western blotting. IgG was used as a control in the IP. β-actin was used as a loading control.

Immunohistochemistry (IHC) and EM

Immunohistochemistry was performed as previously described with slight modification.[63] Mice were anesthetized with 5% isoflurane and transcardially perfused with 0.1 M PBS and 4% paraformaldehyde (PFA) in 0.1 M PBS (pH 7.4). To minimize the variances in fixation, the amount of PBS or 4% PFA used for perfusion was controlled as same amount (ml) of body weight. Brain samples were dissected out and post-fixed in 4% PFA for 4 h at 4°C, and slices into 50-μm-thick sections (with 100 μm apart) by a vibrotome (VT1000S, Leica Biosytems). Brain slices were blocked in 10% donkey serum at room temperature for 1 h and treated in 0.2% Triton X-100 (0.05% Triton X-100 for Immuno-EM) in PBS at room temperature for 30 min. After staining with primary and secondary antibodies (STAR Methods), sections were counterstained with DAPI. For EM, in Figure 2M, anti-mouse IgG-peroxidase (1:1000) in Figure 6A, anti-rat IgG-peroxidase (1:1000,) were used as secondary antibodies. The signal was visualized using a diaminobenzidine (DAB) nickel substrate.[63] DA axons were identified by the deposit of dark signal from TH immunoreactivity in EM.

Please cite this article in press as: Cui et al., In *trans* neuregulin3-Caspr3 interaction controls DA axonal bassoon cluster development, Current Biology (2021), https://doi.org/10.1016/j.cub.2021.05.045

MAP and tissue expansion

Magnified analysis of the proteome (MAP) of synapses was performed as described previously with slight modification.[26] For hydrogel embedding, mice were perfused transcardially with the perfusion buffer containing 5% acrylamide (AA), 0.05% bis-acrylamide (BA), 0.8% sodium acrylate (SA), and PBS, followed by the fixative solution containing 4% PFA, 30% AA, 0.05% BA, 10% SA, 0.1% V-50, and PBS. Brains were dissected and incubated in the fixative solution at 4°C for 24 h and sliced into 1-mm-thick sections using a vibrotome. Sections were incubated in the fixative solution for another 24 h. After a brief wash with PBS, slices were incubated with 1% acetamide (w/v), 1% glycine (w/v), 0.02% NaN (w/v) in H_2O (pH 9.0) at 37°C overnight. Slices were then incubated with the MAP solution (30% AA, 0.1% BA, 10% SA, 0.05% V-50 in PBS) at 4°C for 48 h and 45°C for 2 h. For denaturation, 1-mm-thick hydrogel-embedded sections were cut into 80-μm-thick sections using vibrotome. The resulting sections were incubated in the denaturation solution (200 mM SDS, 200 mM NaCl, and 50 mM Tris in H_2O, pH 9.0) at 37°C with gentle shaking for 2 h and then at 95°C for 45 min. After denaturation, sections were washed with 0.2% Triton X-100 in PBS for 3 times (5 min each) and blocked in 10% donkey serum for 1 h at room temperature. After incubation with primary antibody against TH and bassoon (STAR Methods) for 24 h at room temperature, sections were washed and incubated with secondary antibodies conjugated with Alexa 488 and Alexa 594, respectively for 6 h at room temperature (STAR Methods). Sections were also counterstained with DAPI. For full expansion of the tissues, sections were incubated in 50 mL H_2O at room temperature for 12–48 h with gentle shaking and the water was changed every 3–5 h.

Imaging and data processing

All image data were acquired and analyzed under the same parameters between groups. Imaging data were acquired by a ZEISS LSM 880 system equipped with a 63 × 1.42 N.A. oil immersion objective and 2D Superresolution mode for Airyscan.[64] Z stack images were collected with a step of 150 nm and 20 images and processed using the deconvolution algorithm and 3D processing. Images were acquired from the surface of sections (~5 μm) where antibodies penetration was sufficient. Regions of interest (ROIs) were acquired from ventral NAcc (AP: 1.6 mm) with an imaging volume of 50.7 × 50.7 × 3.0 μm. Data were processed with Gaussian filter and background subtraction before further processing. The background threshold in each channel was obtained by staining brain sections with secondary antibodies without primary antibodies against TH and BSN. To quantify DA axonal density in the NAcc, image stacks of TH staining were filtered with 3D Gaussian filtering, and 3D surface construction of TH+ axons was generated by Imaris.

To quantify TH+BSN+ puncta, MAP treated sections were imaged with 2D super-resolution mode for Airyscan. Data were imported to Imaris 9.5.0 (Bitplane, Zurich, Switzerland). TH (red) and BSN (green) channels were built into independent 3D surfaces. To identify BSN+ puncta within TH+ axons, 3D rendered surface objects of BSN+ puncta were filtered by the shortest distances to TH+ axons surface (≤0.15 μm). Expansion factor (E) was calculated by the quantification of the volume of the nucleus using DAPI staining after the tissue expansion divided by the volume of DAPI before the tissue expansion. To exclude the difference in expansion between samples, TH+BSN+ puncta were built to an independent channel for quantification of volume and normalized with the volume of TH. The volume of TH+BSN+ puncta was normalized with the volume of TH to exclude the difference in expansion.

$$Normalized\ volume\ of\ TH\ +\ BSN+puncta=\frac{(\text{Raw volume of TH}+\text{BSN}+\text{puncta})\times \text{E}}{(\text{Raw volume of TH})\times \text{E}}$$

To characterize the TH+BSN+ double-positive puncta contacting GFP labeled MSNs in the iontoporation experiments (Figure 7), TH+BSN+ puncta were identified by the 3D reconstruction of each channel and filtered by the distance between TH+ axons and BSN+ puncta (distance ≤ 150 nm). To quantify DA synapse onto MSN neurons in different regions, putative DA synapse were identified by TH+BSN+. The distance of TH+BSN+ puncta within 150 nm of the GFP (MSN) signal was filtered and quantified. TH+BSN+ puncta onto spines (< 150 nm) were labeled as axospinous synapses, on dendrite were identified as axodendritic synapses (< 150 nm). To exclude the difference in expansion, the number of DA axonal BSN clusters were normalized with the volume of MSN (GFP) in the region of interest (ROI).

$$Normalized\ number\ of\ DA\ synapses\ =\frac{\text{number of TH}+\text{BSN}+\text{puncta}}{\text{volume of MSN}}$$

In situ hybridization

In situ hybridization was performed as described previously with slight modification.[65] P60 mice were perfused transcardially with 4% PFA in PBS, and the dissected brains were fixed overnight at 4°C in 4% PFA. Brains were then cut to 60 μm coronal sections using a vibrotome in RNase free solutions and incubated with digoxigenin-labeled (DIG) RNA probes at 55°C for 15 h. For probe synthesis, partial DNA between exon 2 and exon 8 (from 1125 - 2052 of murine *Nrg3* mRNA, GenBank: NM_008734) was amplified by primers: forward, 5′-AACAT ACTCC ACTGA ACGAT-3′, reverse 5′-GATGA TGGGC ACAGA ATTG-3′) and subcloned into pGEM-T Vector (A3600, Promega, WI, USA). Resulting plasmid was used as template in PCR (with DIG RNA Labeling Kit, 11175025910, Sigma-Aldrich, MO), for anti-sense and sense cRNA, with T7 and Sp6 primers, respectively. After hybridization, sections were blocked for endogenous peroxidase with 3% H_2O_2, washed with 0.1% Tween20 in PBS, and incubated with donkey anti-DIG-HRP (1:1000, NEL741001KT, PerkinElmer, MA, USA) and anti-TH antibody (1:500, sc-25269, Santa Cruz, CA) at 4°C overnight. After the addition of tyramide-conjugated with fluorescein in the reaction buffer, samples were incubated for 10 min to develop the *Nrg3* mRNA signal. After that, donkey anti-mouse IgG-AlexaFluor594 (1:1000, 711-585-152, Jackson ImmunoResearch) was added to visualize the signal of TH.

Please cite this article in press as: Cui et al., In *trans* neuregulin3-Caspr3 interaction controls DA axonal bassoon cluster development, Current Biology (2021), https://doi.org/10.1016/j.cub.2021.05.045

Quantitative real-time PCR (qPCR) of mRNAs in tissues and single cells

Total RNA was isolated from tissues containing VTA/SNc using TRIzol (15596018, Thermo Fisher Scientific, MA) and cDNA was synthesized using a cDNA synthesis kit (A5000, Promega, WI, USA). In some experiments, the cytoplasm of DA neurons was collected by glass electrodes after patch-clamp recording. mRNA was reverse transcripted using the SuperScript III cDNA Synthesis System (18080300, Thermo Fisher Scientific, MA). qPCR was performed with the SYBR Green qPCR master mix (204056, QIAGEN, Germany) on StepOnePlus real-time PCR system (Thermo Fisher Scientific, MA) with Gapdh as an internal control. See Table S4 for primers.

Purification and conjugation of Caspr3-ECDs

pCDNA3.1 vector encoding Fc-tagged ECD of *Caspr3* (Caspr3-ECD-Fc) was a gift from Dr. Yasushi Shimoda. Human Fc, Caspr3-ECD-Fc, Caspr3-ECD-Fc$^{\Delta LamG1}$ were purified and conjugated to protein A/G beads as previously described.[66] Briefly, HEK293T cells were transfected with pCDNA3.1-Fc, pCDNA3.1-Caspr3-ECD-Fc or pCDNA3.1- Caspr3-ECD-Fc$^{\Delta LamG1}$, and cultured in IgG-low medium. The conditioned medium was collected 24 h and 48 h after conditioning and pooled together. 500 μL protein A/G beads were prewashed using cold PBS three times and incubated with Fc, Caspr3-ECD-Fc$^{\Delta LamG1}$ or Caspr3-ECD-Fc conditioned medium (5 ml) overnight on a rotating shaker at 4°C. Beads were then washed three times with cold PBS and suspended in neuron maintenance medium (1:100). Fc, Caspr3-ECD-Fc$^{\Delta LamG1}$ or Caspr3-ECD-Fc conjugated beads were used for cell aggregation assay.

Cell aggregation assay

Cell aggregation experiments were performed as described before with slight modification.[67] HEK293T cells were plated in 6-well plates, transfected with Flag-Caspr3, LAP-neurexin-1β, NLGN2A, and Nrg3-GFP. 48 h later, cells were digested using 0.05% trypsin-EDTA (GIBCO, 2053593) and suspended with DMEM which contained with 10% FBS, 10 mM CaCl2, 10 mM MgCl2, and 50 mM HEPES-NaOH, pH 7.4 and incubated at room temperature for 1 h under gentle agitation in the presence or absence of Caspr3-ECDs (to disrupt the NRG3-Caspr3 interaction). Cell aggregates were quantified in a new 6-well plate under fluorescence microscopy (BZ-X800, Keyence, Japan).

Slice electrophysiology and Single-unit recordings

Slice preparation and recordings in DA neurons were performed as previously described.[68] Mice (4 to 5-weeks-old males and females) were anesthetized with isoflurane and were subjected to cardiac perfusion with ice-cold oxygenated (95% O_2 and 5% CO_2) artificial cerebrospinal fluid (ACSF, 110 mM choline chloride, 2.5 mM KCl, 0.5 mM $CaCl_2$, 7 mM $MgCl_2$, 1.3 mM NaH_2PO_4, 25 mM $NaHCO_3$, and 20 mM D-glucose) before decapitation. Brains were rapidly removed and cut into blocks that were placed in ice-cold oxygenated ACSF. Horizontal slices (300 μm) containing the midbrain were prepared using a vibrotome (VT1200S, Leica, Germany). Slices were incubated at 32°C for 30 min in a chamber containing recording ACSF (125 mM NaCl, 2.5 mM KCl, 2 mM $CaCl_2$, 1.3 mM $MgCl_2$, 1.3 mM NaH_2PO_4, 25 mM $NaHCO_3$, and 10 mM D-glucose), and they were kept at room temperature for use within 5 h. Recordings were performed in a heated chamber (32°C) that was perfused with recording ACSF at a rate of 3.0 mL/min. To examine the intrinsic electric property, neurons were recorded by whole-cell patch-clamp configuration using a MultiClamp 700B amplifier (10 kHz low-pass Bessel filter and 10 kHz digitization, Molecular Devices, CA) with pClamp 10.7 software (Molecular Devices). Glass electrodes were filled with a solution containing: 125 mM K-gluconate, 10 mM HEPES, 5 mM KCl, 10 mM sodium phosphocreatine, 0.2 mM EGTA, 4 mM Na_2ATP, 0.3 mM Na_3GTP and 4 mM $MgCl_2$, pH 7.2–7.3 and 285–290 mOsm. The series resistance of glass electrodes was not compensated but maintained < 20 mΩ. Input and series resistance were continually monitored; if either parameter changed by > 20%, data were excluded for analysis. Intrinsic properties were calculated based on current clamp responses to a series of 2 s current pulse injections from −300 to 300 pA (50 pA/increment). Input resistance was calculated from the voltage response to a −50 pA, 2 s current pulse. Electrophysiological data were analyzed with Clampfit software and MATLAB (MathWorks, Natick, MA). For analysis of firing rates, spike events were placed in 10 s bins for 3 min. Neurons were excluded from analysis if they showed > 5% variation in firing over time.

Single unit recordings of DA neurons were performed as described previously with slight modification.[63] Briefly, extracellular glass electrodes were pulled from glass tubing (1B150F, World Precision Instruments, FL). The electrodes were filled with 2 M NaCl and 2% biocytin with resistance set to ~15 MΩ. Putative DA neurons were identified according to the previous report.[69] 1) firing rate from 3 to 12 Hz, 2) spike width around 4 ms, 3) burst firing pattern. Recording sites in the VTA region was identified by biocytin labeling by postmortem analysis. Recorded data were submitted to spike sorting, to identify single-unit clusters using Klusters and NeuroScope.[70] Bursty activity in DA neurons was defined based on ISI (80 - 160ms).[71] Bursty DA neurons were identified by ISI last 80 - 200 ms.[72] The categorization of DA neurons into bursty or non-bursty based on ISI was conducted by two lab members blind to genotypes. Analyses of unit data were conducted using home-made scripts for MATLAB.

FSCV

Fast scanning cyclic voltammetry (FSCV) recording in anesthetized animals was performed as described previously.[62] Glass-encased carbon fiber electrodes were made by inserting a 7 μm carbon fiber (T650, Goodfellow Corporation, PA, USA) into a glass tubing (1B150F, World Precision Instruments, FL, USA). To increase the sensitivity, electrodes were soaked in isopropanol for > 10 min. Electrodes were scanned at 60 Hz for 30 min using a triangular scanning waveform from −0.4 V (versus Ag/AgCl) to 1.3 V and back to −0.4 V at a scan rate 400 V/s, to increase the stability of baseline and sensitivity. Ag/AgCl electrodes (E255A, *In Vivo*

Metric, CA, USA) were used as the reference. Finally, glass electrodes were tested *in vitro* for noise level (< 0.1 nA) and sensitivity with standard concentrations of DA (25-100 nM) using a flow injection system.[73]

Mice were anesthetized animals (2.5% isoflurane in a 30%:70% O_2: N_2 gas mixture), to minimize the effect of emotion and movement.[74] Anesthetized mice were placed on a heating pad to maintain the body temperature at 37°C, and mounted to a stereotactic apparatus in a Faraday cage. Holes were drilled in the skull (Bregma 1.1mm anteriorly, 1.1 mm laterally), glass-encased carbon fiber electrodes were inserted into ventral NAcc for DA transients recording. To characterize activity-dependent DA release and to obtain the training sets of principal component regression (PCR), a stimulating electrode was inserted in the medial forebrain bundle (MFB) (AP: −1.3 mm, ML: 1.20 mm, DV: 4.90 mm). A reference electrode was placed in the dura above the cerebellum. After stabilization for 10 min, spontaneous DA transients were usually detectable and will be recorded for 10 trials, each for 1 min. *In vivo* recording signals were acquired with a PCIe card (NIPXIe-6363, National Instruments, TX, USA) and analyzed by a LabVIEW software.[75] In some experiments, mice were injected with raclopride (1 mg/kg, or 5 mg/kg, i.p.) and recorded for spontaneous DA transients. Activity-elicited DA release was recorded in response to a train of pulses (48 pulses, 60 Hz, 100 μA) that was delivered by the stimulating electrode. After recording, electrolytic lesion current was applied through glass electrodes to label recording sites in the NAcc, which was examined by postmortem analysis. For each mouse, after recording DA transients, training sets of DA and pH data were obtained by MFB stimulation. After PCR analysis, DA concentration was extracted and analyzed using MATLAB scripts. For DA recording in brain slices, experiments were done based on the previous study.[34] Coronal brain slices containing NAcc was prepared as the slice electrophysiology. 100 nM DHβE was added to the ACSF (see above). Carbon fiber electrodes were placed in NAcc region. DA release was elicited by a bipolar concentric electrode (FHC, USA) about 100 μm from the carbon fiber electrodes at 60 Hz. Peaks of evoked DA release were extracted and analyzed using MATLAB scripts (STAR Methods).

DA and 5-HT measurement

Monoamines were measured as previously described.[76] Standard solutions of DA and 5-HT were prepared in water at concentrations from 1 ng/mL to 500 ng/mL including 200 ng/mL phenylalanine-d5 (internal standard). Internal standard (40 ng/mL) or brain homogenates (100 μl) were mixed with 400 μl methanol containing and centrifuged at 18000 *rcf* for 10 min. 350 μl supernatant was transferred to glass test tubes, dried under N2 flow, and dissolved by 70 μl of water for HPLC analysis. Dopamine and 5-HT were analyzed using the TSQ Quantiva Triple-Stage Quadrupole Mass Spectrometer (Thermo Fisher Scientific). Standards and brain homogenate extract samples were loaded to a C18 column (Gemini, 3 μm, 2 × 150 mm, Phenomenex) for separation. Mobile phase A consisted of a water/formic acid (100/0.2 by volume); mobile phase B consisted of a methanol/formic acid (100/0.2 by volume). A linear gradient was generated at 0.3 mL/min: 0 - 2 min, 0% B; 2 - 8 min, 0%B to 100%B; 8-12 min, 100%B; 12-12.1 min, 100%B to 0%B, 12.1-18 min, re-equilibrate with 0% B. The injection volume was 5 μl controlled by an autosampler (UltiMate ACC-3000, ThermoFisher). The column was controlled by a 25C, and the auto-sampler compartment was set to 4C. The HPLC eluent was automatically injected onto the Quantiva and ionized with electrospray ionization in positive mode. Both the dopamine and 5-HT were monitored using selected reaction monitoring (SRM) mode. The SRM transitions (m/z) were 154 → 91 for dopamine, 177 → 115 for 5-HT, and 171 → 106 for the internal standard phenylalanine-d5. The quantity of dopamine and 5-HT in brain homogenate was calculated using the internal calibration curves and normalized with the protein concentration in the brain homogenate.

QUANTIFICATION AND STATISTICAL ANALYSIS

Data are presented as mean ± SEM unless specified otherwise. Sample sizes were chosen based on power analysis using G*Power3.1.9.6.[77] Data were analyzed by two-tailed Student's t test (two groups of data) and one-way ANOVA followed by Tukey's post hoc test for multiple comparisons (3 or more groups of data) using SPSS Statistics 19 software (IBM, Armonk, NY, USA). Significance was defined as * $p < 0.05$. All the description of statistical information can be found in the figure legends

Current Biology, Volume *31*

Supplemental Information

In *trans* neuregulin3-Caspr3 interaction controls DA axonal bassoon cluster development

Wanpeng Cui, Nannan Gao, Zhaoqi Dong, Chen Shen, Hongsheng Zhang, Bin Luo, Peng Chen, Davide Comoletti, Hongyang Jing, Hongsheng Wang, Heath Robinson, Wen-Cheng Xiong, and Lin Mei

Figure S1

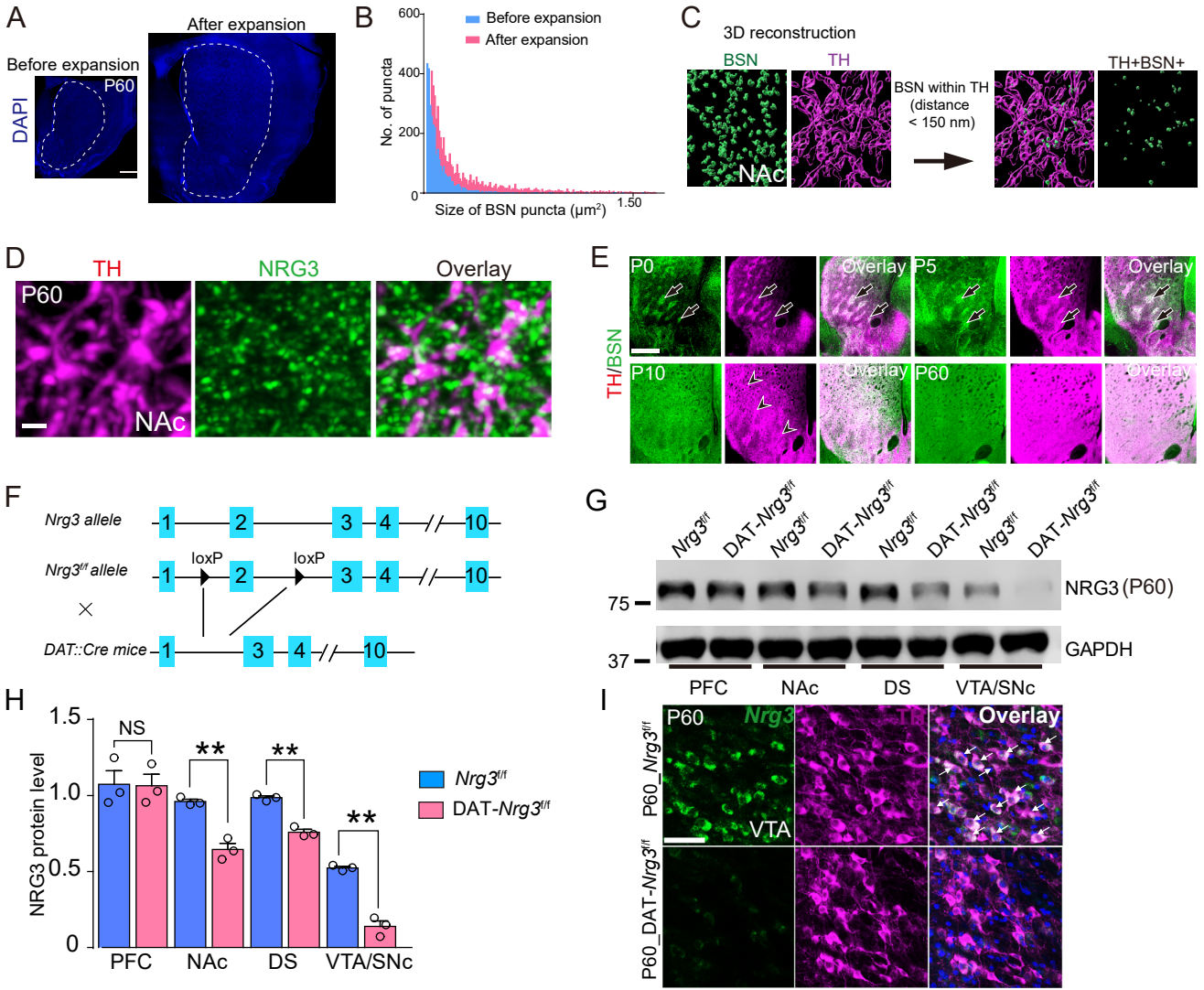
A
After expansion
Before expansion
DAPI
P60
B
Before expansion
After expansion
No. of puncta
600
400
200
0
1.50
Size of BSN puncta (μm²)
C
3D reconstruction
BSN
TH
TH+BSN+
BSN within TH
(distance
< 150 nm)
NAc
D
TH
NRG3
Overlay
P60
NAc
E
P0
P5
P10
P60
Overlay
TH/BSN
F
Nrg3 allele
Nrg3f/f allele
loxP
DAT::Cre mice
1
2
3
4
10
G
Nrg3f/f
DAT-Nrg3f/f
75
37
NRG3 (P60)
GAPDH
PFC
NAc
DS
VTA/SNc
H
NRG3 protein level
1.5
1.0
0.5
0
NS
**
PFC
NAc
DS
VTA/SNc
Nrg3f/f
DAT-Nrg3f/f
I
P60
Nrg3
TH
Overlay
VTA
P60_Nrg3f/f
P60_DAT-Nrg3f/f

Figure S1. Characterization of NRG3 expression pattern in postnatal stages, and generation of DAT-*Nrg3*$^{f/f}$ conditional knockout mice, Related to Figure 1

(A) Coronal brain slices containing striatum were stained with DAPI before (left in A) and after MAP (middle in A). Scale bar, 500 μm.

(B) Size of BSN clusters before (blue) and after expansion (red). Kolmogorov-Smirnov test, $p < 0.0001$.

(C) Quantification of the TH+BSN+ puncta in stratum by closest distance calculation. BSN puncta (green in C) and DA axons (TH, purple in C) after MAP and airyscan were 3D reconstructed in Imaris. Scale bar, 5 μm.

(D) Enrichment of NRG3 in the axonal of DA neurons. DA axons were identified by immunohistochemistry of TH (magenta in D), and NRG3 (green in D) was visualized using an anti-NRG3 antibody in the NAc region of coronal brain sections from WT animals. Arrows indicate TH+NRG3+ puncta. Scale bar, 3 μm.

(E) Colocalization of DA axons (TH, magenta in E) with BSN (green in E) in early postnatal stages (P0 - P5), but not P10 and P60. Arrows indicate colocalization of DA islands with BSN. Arrowheads indicate DA island in P10. Scale bar, 500 μm.

(F) Schematic diagram showing the generation of DAT-*Nrg3*$^{f/f}$ conditional knockout mice. *Nrg3*$^{f/f}$ mice were crossed with a *DAT*::*Cre* knock-in line, exon2 of *Nrg3* was deleted by Cre recombinase.

(G) Reduced expression of NRG3 in NAc, Ds and VTA/SNc of DAT-*Nrg3*$^{f/f}$ mice. Shown are representative blots of NRG3 and GAPDH from three independent experiments.

(H) Quantitative analysis of NRG3. NRG3 level of *Nrg3*$^{f/f}$ mice in PFC were taken as 100%. PFC from *Nrg3*$^{f/f}$ (1.07 ± 0.09) vs. DAT-*Nrg3*$^{f/f}$ (1.06 ± 0.08) mice, $p = 0.93$; NAcc from *Nrg3*$^{f/f}$ (0.96 ± 0.02) vs. DAT-*Nrg3*$^{f/f}$ (0.65 ± 0.04) mice, $p = 0.0018$; DS from *Nrg3*$^{f/f}$ (0.99 ± 0.01) vs. DAT-*Nrg3*$^{f/f}$ (0.75 ± 0.02) mice, $p = 0.0005$; VTA/SNc from *Nrg3*$^{f/f}$ (0.54 ± 0.01) vs. DAT-*Nrg3*$^{f/f}$ (0.14 ± 0.03) mice, significant effect of genotype, $F_{(1,16)} = 50.70$, $p < 0.0001$, Two-way ANOVA with Sidak's post hoc. n = 3 for each group. ** $p < 0.01$. Data are mean ± SEM.

(I)Representative images showing ISH of *Nrg3* mRNA (green in H) and immunohistochemistry of TH (magenta in H) in the VTA/SNc region. Scale bars, 100 μm. Arrows indicate TH+*Nrg3*+ cells.

Figure S2

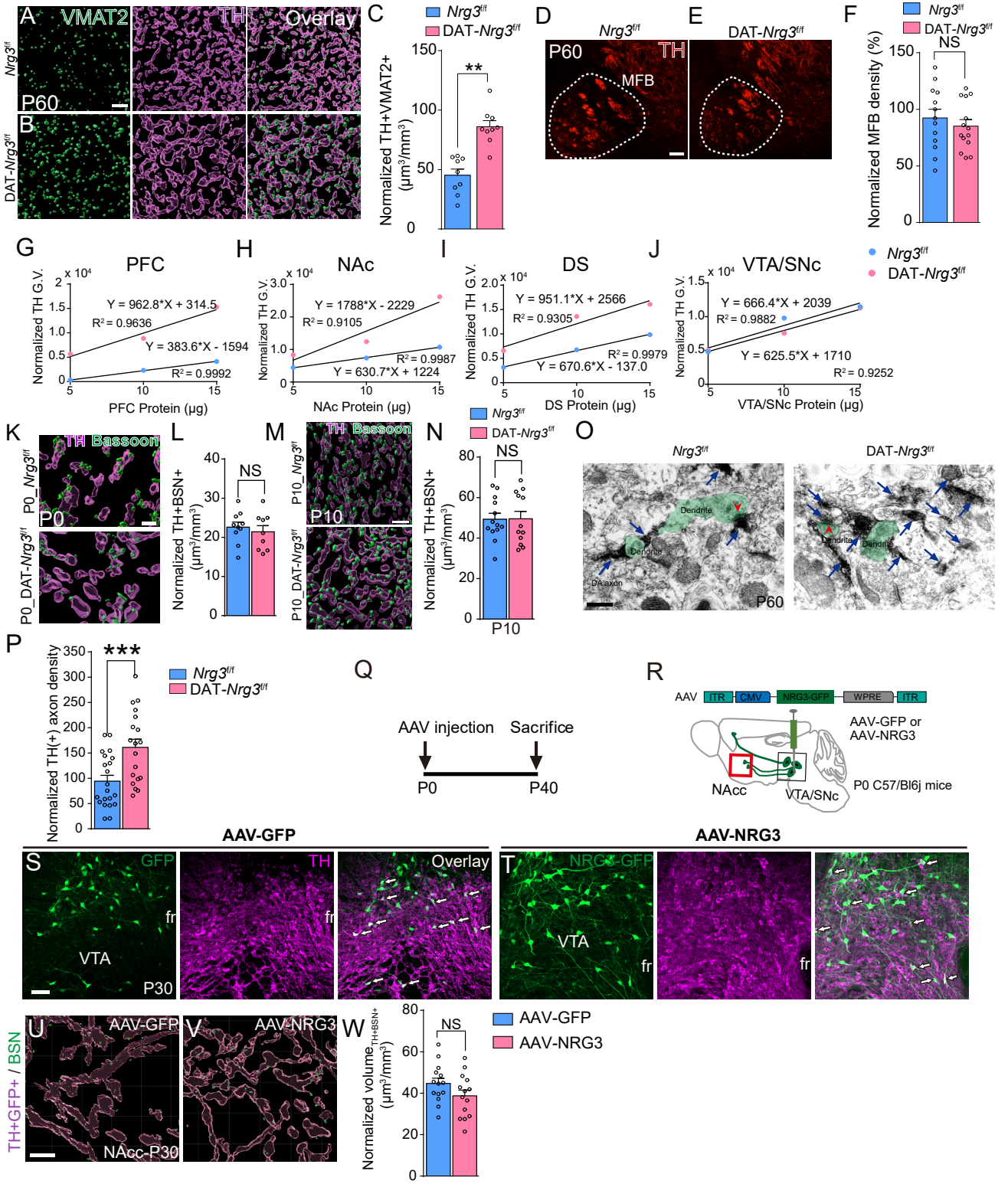
A
VMAT2
TH
Overlay
Nrg3f/f
P60
B
DAT-Nrg3f/f
C
Nrg3f/f
DAT-Nrg3f/f
Normalized TH+VMAT2+ (μm3/mm3)
**
D
Nrg3f/f
P60
TH
MFB
E
DAT-Nrg3f/f
F
Nrg3f/f
DAT-Nrg3f/f
NS
Normalized MFB density (%)
G
PFC
x 10^4
Normalized TH G.V.
Y = 962.8*X + 314.5
R2 = 0.9636
Y = 383.6*X - 1594
R2 = 0.9992
PFC Protein (μg)
H
NAc
Y = 1788*X - 2229
R2 = 0.9105
R2 = 0.9987
Y = 630.7*X + 1224
NAc Protein (μg)
I
DS
Y = 951.1*X + 2566
R2 = 0.9305
R2 = 0.9979
Y = 670.6*X - 137.0
DS Protein (μg)
J
VTA/SNc
Y = 666.4*X + 2039
R2 = 0.9882
Y = 625.5*X + 1710
R2 = 0.9252
VTA/SNc Protein (μg)
Nrg3f/f
DAT-Nrg3f/f
K
TH Bassoon
P0_Nrg3f/f
P0
P0_DAT-Nrg3f/f
L
NS
Normalized TH+BSN+ (μm3/mm3)
M
TH Bassoon
P10_Nrg3f/f
P10
P10_DAT-Nrg3f/f
N
Nrg3f/f
DAT-Nrg3f/f
NS
P10
O
Nrg3f/f
DAT-Nrg3f/f
Dendrite
DA axon
P60
P
***
Nrg3f/f
DAT-Nrg3f/f
Normalized TH(+) axon density
Q
AAV injection
Sacrifice
P0
P40
R
AAV
ITR
CMV
NRG3-GFP
WPRE
ITR
AAV-GFP or
AAV-NRG3
NAcc
VTA/SNc
P0 C57/Bl6j mice
AAV-GFP
AAV-NRG3
S
GFP
TH
Overlay
fr
VTA
P30
T
NRG3-GFP
VTA
fr
U
AAV-GFP
NAcc-P30
V
AAV-NRG3
TH+GFP+ / BSN
W
NS
Normalized volume TH+BSN+ (μm3/mm3)
AAV-GFP
AAV-NRG3

Figure S2. Increased TH+VMAT2+ puncta, no change in the volume of medial forebrain bundles (MFB) in DAT-*Nrg3*$^{f/f}$ mice, Related to Figure 2

(A-B) Representative 3D reconstructed images showing TH (purple in A) and VMAT2 (green in B) in the NAcc after MAP processing. Scale bar, 7 μm.

(C) Quantification of TH+VMAT2+ density in A and B. Volume of TH+VMAT2+ puncta were normalized with the volume of TH. $p < 0.01$, $t = 6.375$, Student's *t* test.

(D-E) Representative images of MFB from P60 mice. TH (Red in D and E). Scale bar, 100 μm.

(F) Quantification in H and I. Data was normalized with MFB volume of *Nrg3*$^{f/f}$ group. $p = 0.4579$, $t = 0.7540$, Student's *t* test. n = 13-14 mice from *Nrg3*$^{f/f}$ and DAT-*Nrg3*$^{f/f}$ mice respectively.

(G-J) Quantification of TH in Figure 2A. PFC, Pearson r = 0.9996 for *Nrg3*$^{f/f}$ and r = 0.9816 for DAT-*Nrg3*$^{f/f}$. NAc, Pearson r = 0.9994 for *Nrg3*$^{f/f}$ and r = 0.9542 for DAT-*Nrg3*$^{f/f}$. DS, Pearson r = 0.9990 for *Nrg3*$^{f/f}$ and r = 0.9646 for DAT-*Nrg3*$^{f/f}$. VTA, Pearson r = 0.9619 for *Nrg3*$^{f/f}$ and r = 0.9941 for DAT-*Nrg3*$^{f/f}$.

(K) Representative 3D reconstructed images of TH and BSN in NAcc at P0 after MAP. Scale bar represents 5 μm.

(L) Quantification of normalized volume of TH+BSN+ in K. $p = 0.5672$, $t = 0.5835$, Student's *t* test. n = 9 - 10 slices from 3 mice for each genotype.

(M) Representative 3D reconstructed images of TH and BSN in NAcc from *Nrg3*$^{f/f}$ (top) and DAT-*Nrg3*$^{f/f}$ (bottom) mice at P10 after MAP. Scale bar represents 7 μm.

(N) Quantification of normalized volume of TH+BSN+ clusters in M. $p = 0.9640$, $t = 0.04536$, Student's *t* test. n = 12 slices from 3 *Nrg3*$^{f/f}$ mice, and n = 13 slices from 3 DAT-*Nrg3*$^{f/f}$ mice. NS, not significant.

(O) Representative images of immuno-EM study. DA axons were visualized by HRP reaction of TH. Red arrow heads, postsynaptic density. Light green shade, putative dendrites. Scale bar, 200 nm.

(P) Quantification in O. ***$p = 0.0015$, Student's *t* test, $t = 3.426$, 19-21 slices from 3 mice for each group. Data, mean ± SEM.

(Q-R) Experimental design of AAV-NRG3-GFP injection in VTA.

(S-T) Representative images showing expression of GFP and NRG3-GFP in the DA neurons in VTA. Cells expressing GFP (green in S and T) were co-stained with TH (magenta in S and T) to identify the DA neurons transfected. Arrows indicate the DA neurons. Scale bars represents 50 μm.

(U-V) No alteration of DA axonal BSN clusters after overexpression of NRG3 in DA neurons. TH and GFP axons (purple in U and V), BSN (green in U and V). Scale bar 2 μm.

(W) Quantification of density of TH+BSN+ puncta in U and V. $p = 0.1198$, $t = 1.608$. n = 14 slices from 3 mice for each group. NS, not significant. Student's *t* test.

Figure S3

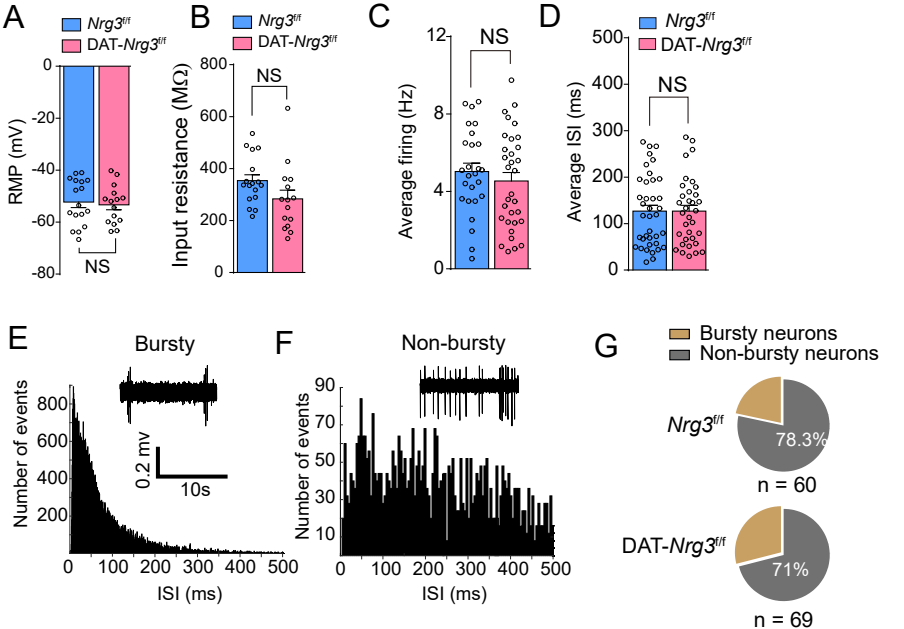
A
Nrg3f/f
DAT-Nrg3f/f
RMP (mV)
0
-20
-40
-60
-80
NS
B
Nrg3f/f
DAT-Nrg3f/f
Input resistance (MΩ)
800
600
400
200
0
NS
C
Average firing (Hz)
12
8
4
0
NS
D
Nrg3f/f
DAT-Nrg3f/f
Average ISI (ms)
500
400
300
200
100
0
NS
E
Bursty
Number of events
800
600
400
200
0.2 mv
10s
0
100
200
300
400
500
ISI (ms)
F
Non-bursty
Number of events
90
70
50
30
10
0
100
200
300
400
500
ISI (ms)
G
Bursty neurons
Non-bursty neurons
Nrg3f/f
78.3%
n = 60
DAT-Nrg3f/f
71%
n = 69

Figure S3. Increased evoked DA release in the NAcc of DAT-*Nrg3*$^{f/f}$ mice, and no difference in resting membrane potential and input resistance in DA neurons if DAT-*Nrg3*$^{f/f}$ mice, Related to Figure 3

(A-B) No alteration in resting membrane potential (RMP) and input resistance. t = 0.3792 for RMP, and t = 1.776 for input resistance. n = 17 neurons from 3 *Nrg3*$^{f/f}$ mice, n = 15 neurons from 3 DAT- *Nrg3*$^{f/f}$ group. Bar graphs represent mean ± SEM. Student's t test. NS, not significant

(C) Similar overall firing rate of putative DA neurons between *Nrg3*$^{f/f}$ and DAT-*Nrg3*$^{f/f}$ mice in the single-unit recording. $p = 0.4364$, $t = 0.7839$, Student's *t* test.

(D) Quantitative analyses of interspike interval (ISI) of putative DA neurons. $p = 0.9996$, $t = 0.0005$, Student's *t* test.

(E-F) Representative ISI histograms by single-unit recordings. Insets, raw traces of action potentials. Scale bar, 10 s, 0.2 mV.

(G) No difference in population of bursty or non-bursty neurons between *Nrg3*$^{f/f}$ (left, n = 60 neurons) and DAT-*Nrg3*$^{f/f}$ (right, n = 69 neurons) mice.

Figure S4

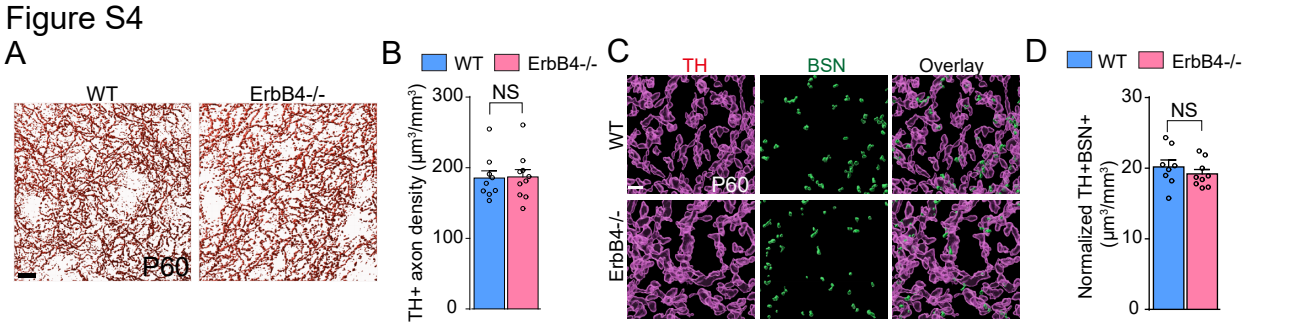
A
WT
ErbB4-/-
P60
B
WT
ErbB4-/-
NS
TH+ axon density (μm³/mm³)
300
200
100
0
C
TH
BSN
Overlay
WT
ErbB4-/-
P60
D
WT
ErbB4-/-
NS
Normalized TH+BSN+ (μm³/mm³)
30
20
10
0

Figure S4. No alteration in the number of DA axonal BSN clusters in ErbB4-/- mice, Related to Figure 5

(A-B) Loss of ErbB4 did not promote DA axon arborization in ErbB4-/- mice. Representative 3D surface reconstruction of TH+ DA axons in NAcc from WT and ErbB4-/- mice respectively. DA axons in NAcc were identified by antibody again TH. Scale bar in A, 5 μm.

(B) Quantification of volume of DA axons in D. p = 0.8835, t =0.1488, n = 9 slices from 3 WT mice, and n = 10 slices from ErbB4-/- mice. Student's t test. NS, not significant.

(C) No change in the number of DA axonal BSN clusters in adult ErbB4 -/- mice. Representative 3D reconstructed images of TH (purple in C), and BSN (green in C) after tissue expansion in WT or ErbB4-/- mice. Scale bar in C, 5 μm.

(D) No change in normalized volume of TH+BSN+ in ErbB4-/- mice. p = 0.3958, t = 0.8741. n = 8 - 9 slices from 3 WT and 3 ErbB4-/- mice. Student's t test.

Figure S5

A

B

Caspr3 sequence
Deletion (red lower case, strike through,278 bp)
Indels (parentheses)

GACAAAATTGGTGCATACGTGCTATGGGATGCCACAGTACCAGGAGA
CTAAGTTTCCGTGAAACTGTTCACCTCGGGACTGTGTCCAGGTTCCTA
AATCTGTCAAGCAAGTCATTACTGGAGTGGATGTAGCAAATAGTAGAT
AATTGAGAAAGCAAAACAAAATTGCTATATCTATGTTAAACATTAGCAA
AACTATTTGAAAGAAGACAGCCTTTT**(ggata)**TAGGCAGAGTGAACACA
TGCCACCATTGA~~tataagctatgataatacaaaaatgatcttgaagatacgttgaccctcctcttt~~
~~gtttttacagggatttccaggaaacacaaatgcagacagtgtggtacaatatagtctccagccttccttcc~~
~~acaccaggttcctgcgcttcctcccctaacctggaacccctaaaggcaggattgggatgcggatagaag~~
~~tatatgggtgttcatacagtaagtgatatttatttttccatgtaaaataaacatctgcatgagatgctgcaaaa~~
~~gccagcgtc~~AGTTAAAAATTACTTGCTCTAGACATTTTTAGTAATTGTATAA
TTAAAACCGA**(gt)**GTTATGAGACTTCTACTAACTCCTTATGACAATATAG
GCTTTAATTATTTTTTTCATAGTTAAATTTAGAGATTGCTTAGTGAGAAA
AATGTTTGATAGGAAATAAGGGTGTAATTTTGGAGCCCTAGTATCACAT
AAAAGGGCAGGTGTACAGTGAATGTCTACGAACCCAGTGCTGGAGAC
AGAGAACAGAGACAGGTAAATCT

C

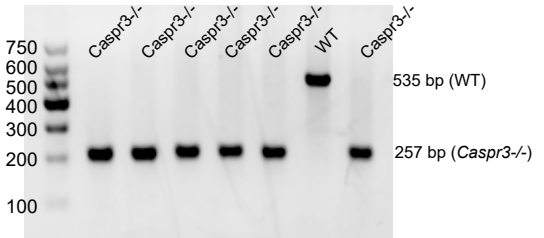

D

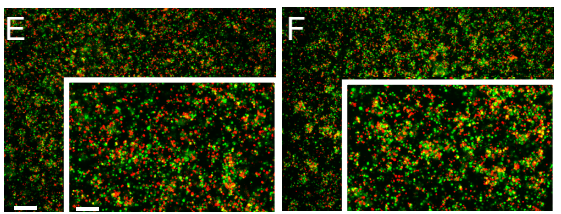

G

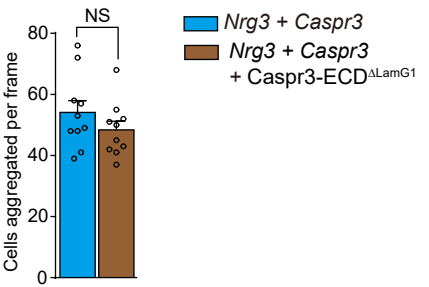

Figure S5. Generation of Caspr3-/- mice, Related to Figure 6

(A-B) Generation of Caspr3-/- mice. (A) Genomic structure of the *Caspr3* allele and Caspr3 null allele. *Caspr3* exon4 was deleted in the Caspr3-/- mice by CRISPR/Cas9 mediated genome editing. (B) DNA sequencing of Caspr3-/- mice showing deletion of 278 bp of DNA (red strike-through) which contains exon4 of *Caspr3*. Two additional deletions, a 5 bp (GGATA) deletion 29 bp before the exon4 deletion and a 2 bp deletion (GT) 53 bp after the 278 bp deletion were found.

(C) Genotyping for WT and Caspr3-/- mutant. PCR results showed a 535 bp band for WT mice, and 257 bp band for Caspr3-/- mice.

(D) Domain organization of Caspr3. ECD of Caspr3 has a region similar to fibrinogen (FRed), four laminin G domains (LamG), two EGF repeats, and a discoidin and the fibrinogen-like domains (DISC). Caspr3 also contains a carboxyl-terminal binding site for PDZ domains.

(E-F) Caspr3-ECD$^{\Delta LamG1}$ did not blocked NRG3-Caspr3 interaction in vitro. Representative images of transcellular adhesion for NRG3 and Caspr3 in HEK293T cells. Cells were transfected with NRG3 or Caspr3; NRG3 or Caspr3 added with Caspr3-ECD$^{\Delta LamG1}$ in the mixture medium. Insets in E and F are high magnification. Scale bars in F, 200 μm, in inset 100 μm.

(G) Quantification of aggregated cells in the data from E and F. n n =10 frames for each group. $p = 0.2469$, t = 1.197, Student's *t* test. All data represent mean ± SEM.

Figure S6

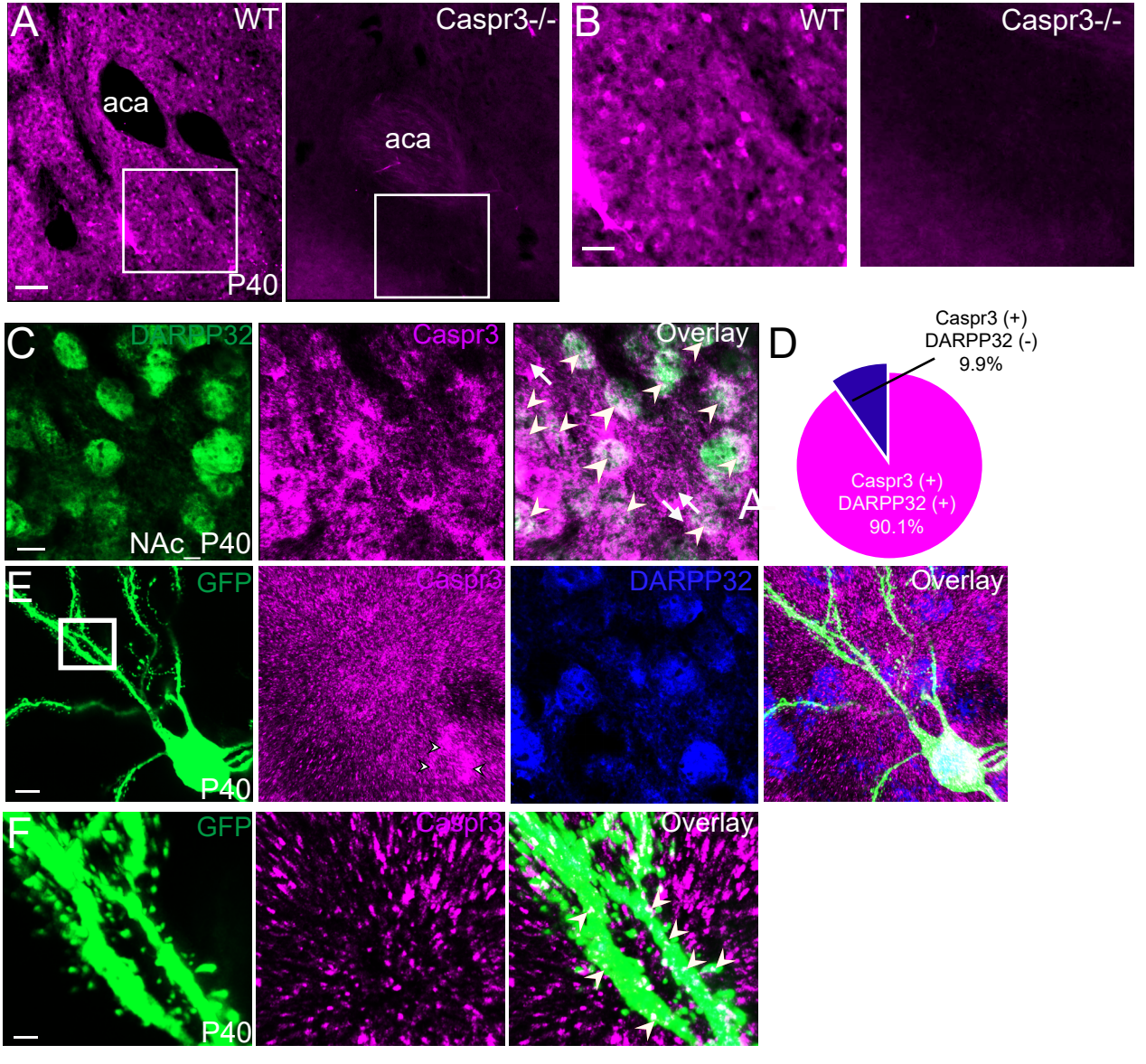
A
WT
aca
P40
Caspr3-/-
aca
B
WT
Caspr3-/-
C
DARPP32
NAc_P40
Caspr3
Overlay
D
Caspr3 (+)
DARPP32 (-)
9.9%
Caspr3 (+)
DARPP32 (+)
90.1%
E
GFP
P40
Caspr3
DARPP32
Overlay
F
GFP
P40
Caspr3
Overlay
MSNs in vivo

Figure S6. Subcellular localization of Caspr3 in MSNs, Related to Figure 6

(A) Representative images showing the expression of Caspr3 in NAc of WT but not Caspr3-/- mice. Caspr3 was visualized by immunohistochemistry using antibody against Caspr3. Scale bar 500 μm.

(B) High magnification of images in A. Scale bar 30 μm.

(C) Representative images showing enrichment of Caspr3 in adult MSNs. MSNs were identified by DARPP32 immunohistochemistry (green in C), and Caspr3 was visualized by antibody against Caspr3 (magenta in C). Arrow heads indicate Caspr3+ cells which are MSNs. Scale bar, 20 μm.

(D) Quantification of Caspr3+ cells in A. 90.1% of Caspr3+ cells are MSNs. n = 707 cells.

(E) Subcellular localization of endogenous Caspr3 in MSNs. Plasmid expressing GFP was electroporated to the striatum of P0 WT mice. MSNs expressing GFP (green in E) were identified by immunostaining with antibodies against DARPP32 (blue in E), Caspr3 was visualized by antibody against Caspr3 (magenta in E). Scale bar in E, 10 μm.

(F) High magnification of images in E showing Localization of Caspr3 in the dendrite shaft of MSNs. Arrow heads indicate the Caspr3 puncta in the dendrites of MSNs. Scale bar in F, 2 μm.

Figure S7

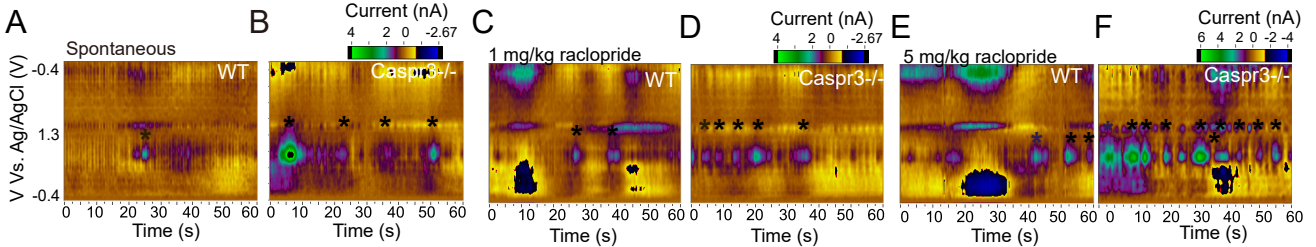
A
Spontaneous
WT
V Vs. Ag/AgCl (V)
-0.4
1.3
-0.4
Time (s)
B
Current (nA)
4 2 0 -2.67
Casper3-/-
Time (s)
C
1 mg/kg raclopride
WT
Time (s)
D
Current (nA)
4 2 0 -2.67
Casper3-/-
Time (s)
E
5 mg/kg raclopride
WT
Time (s)
F
Current (nA)
6 4 2 0 -2 -4
Caspr3+/-
Time (s)

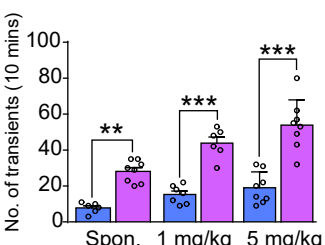
G
No. of transients (10 mins)
Spon.
1 mg/kg
5 mg/kg

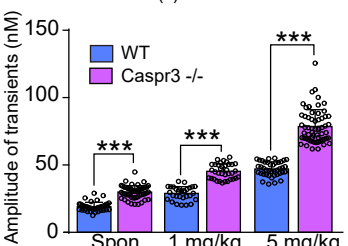
H
Amplitude of transients (nM)
WT
Caspr3 -/-
Spon.
1 mg/kg
5 mg/kg

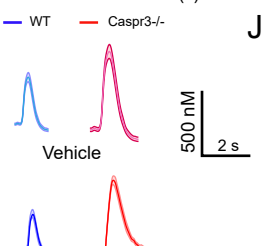
I
WT
Caspr3-/-
Vehicle
500 nM
2 s
DHβE, 100 nM

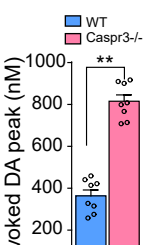
J
WT
Caspr3-/-
Evoked DA peak (nM)

Figure S7. Increased DA transmission in Caspr3-/- mice, Related to Figure 6

(A-B) Increased number of spontaneous DA transients in Caspr3-/- mice. Representative FSCV recordings of spontaneous DA transients in NAcc of WT (A) and Caspr3-/-mice (B). Asterisks indicate spontaneous DA transients.

(C-F) Potentiation of DA transients in NAcc of Caspr3-/- mice by raclopride. Representative FSCV recordings of DA transients 30 min after 1 mg/kg (*i.p.)* raclopride administration in WT (C) and Caspr3-/- (D) during a 1 min session. (E-F) Representative FSCV recordings of DA transients 30 min after 5 mg/kg (*i.p.)* raclopride in NAcc of WT (E) and Caspr3-/- mice (F) in 10 min. Asterisks indicate spontaneous DA transients.

(G) Quantification of number of DA transients in spontaneous condition, 1mg/kg raclopride, or 5 mg/kg raclopride in WT and Caspr3-/- mice in FSCV recordings. ** $p < 0.01$, ***$p < 0.001$. $F_{(5.37)} = 30.00$, One-way ANOVA followed by Tukey's *post hoc*.

(H) Quantification of amplitudes of DA transients in WT and Caspr3-/- mice. Amplitudes of DA transients in spontaneous release, *** $p < 0.001$. $F_{(5.46)} = 427.41$, One-way ANOVA followed by Tukey's *post hoc*. n = 6-7 mice for WT group, n= 6-8 for Caspr3-/- group.

(I) Representative evoked DA peaks in WT and Caspr3-/- mice using brain slices. Brain slices from both WT and Caspr3-/- mice were extracted for FSCV recording *in vitro*. nAchR antagonist, DHβE (100 nM). Electrical stimulation applied at 60 Hz for 0.1 s.

(J) Quantification of peak concentration of DA in I. n = 8 slices from 3 mice for each group. $p = 0.0002$, $t = 10.99$, Student's *t* test. All data represent mean ± SEM

Gene ID	Accession No.	*p* value (P3 VS P10)	*p* value (P60 VS P10)	F value
Nlgn2	*NM_001364137.1*	0.7217	0.1599	1.69048
Nrxn1	*NM_020252.3*	0.9623	0.39	1.38296
Nrxn3	*NM_172544.3*	0.1753	0.101	8.4802
EphB1	*NM_173447.3*	0.7596	0.3338	2.1774
Flrt1	*NM_201411.2*	0.1709	0.405	7.27341
Tenm1	*NM_011855.4*	0.9259	0.2258	3.36215
Tenm2	*NM_011856.4*	0.6451	0.0564	2.5166
Cadm1	*NM_001310841.1*	0.6317	0.2732	2.74189
Ncam1	*XM_006510055.2*	0.3563	0.3243	3.25928
Cdh2	*NM_007664.5*	0.5748	0.1426	4.04793
ERBB4	*XM_006495692.4*	0.9624	0.7848	0.16168
Nrg1	*XM_006509059.4*	0.4363	0.2521	2.25888
Nrg2	*NM_001167891.2*	0.5389	0.0319	1.20063
Nrg3	*NM_008734.3*	0.0244	0.0412	39.359
Rims1	*NM_053270.2*	0.2003	0.2204	4.97241
Rims2	*NM_053271.2*	0.2512	0.3126	5.19655
BSN	*NM_007567.2*	0.3979	0.339	2.24244
TH	*NM_009377.2*	0.3141	0.1717	3.70538
Drd1	*NM_010076.3*	0.0355	0.3998	24.6553
Drd2	*NM_010077.3*	0.1319	0.4262	13.0801
NTN1	*NM_008744.2*	0.9958	0.0688	5.1403

Table S1. Candidate cell adhesion molecules in the regulation of DA neurons development and quantification of mRNA in P0, P10, and adult stages, related to Figure 1.

Candidate cell adhesion molecules used in the mRNA analysis in different postnatal stages by qPCR. n = 3 for each group, One-way ANOVA followed by Tukey's *post hoc*.

NRG3	1	2	3	4	5	6	7	8	9	10	11	12	13	14	15	16	17	18	19	20
A	CBLN 1	NXb	LRRC 3	NRXN 3b	CBLN 2	NRXN 1b	CBLN 3	APOE	CBLN 4	CNTN 1	TM9S F4	CLU	BMP2	SFRP 1	SFRP 2	TNR	NGR N	GPC4	TMEF F2	GPC5
B	SFRP 4	FZD9	NTRK 3	FZD1 0	EPHB 2	PLXN D1	PCDH B4	OPC ML	LPHN 2	LSAM P	RSPO 2	IGLO N5	BGN	SPOC K3	NTN5	NRG3	EPHB 3	ERBB 2	PCDH B13	ERBB 4
C	NEG R1	GPC1	NTRI	GPC3	SFRP 5	GPC6	TMEF F1	CNTN AP2	SFRP 3	CNTN AP2 D2-8	TICN 2	CNTN AP2 D1	NPTX 2	CNTN 2	SPOC K1	RELN D3-6	LRRC 17	RELN D5-6	LRP1 0	RELN D1-2
D	EPOR	MUS K	IL1RA PL2	LRP4	OLFM 4	AGR N	EPHA 7	DGC R2	PCDH B3	TME M108	LRRC 15	Cntn1	VASN	Cntn2	NCST N	Cntn3	FZD3	Cntn4	SDC1	Cntn5
E	OLFM 2	RELN D3-4	ICAM 1	LDLR	PTX4	VLDL R	OLFM 3	LRP8	NYX	RELN D7-8	LRP3	RELN FL	OLFM 1	DGC R2	MYO C	NLGN 1 Y692	EPHB 6	TENM 1	NTN1	LRRT M1
F	ELFN 2	Cntn6	LGI2	Dsca m	CDH5	Dsca ml1	FBLN 1	Islr	EFNA 3	Islr2	VWC 2	Jam1	OLFM L3	Jam2	LING O2	Jam3	NTN3	Jam4	MUC2 0	L1ca m
G	SLITR K6	LRRT M3	SLITR K2	LPHN 1	SLITR K4	NTNG 2	SLITR K1	CNTN AP4	DNER	SALM 5	NTN4	LRRN 1	LRRN 2	PRRT 2	SLITR K5	IGSF 8	ROB O2	SDC3	ASTN 2	LRRN 2
H	LYPD 5	Lrrc4	NPTN	Lrrc4c	NTRK 1	Ncam 1	LING O1	Neo1	CDH1 3	Nrp1	FNDC 7	Nrp2	FZD9	Ntn1	NETO 2	Ntn3	LRRT M1	Ntn4	EPHB 1	Ntn5
I	BCAN	BCAN	MDG A2	CSPG 5	BAI1	TNR	PTPR J	APPα	EGFL AM	APPβ	CNTN 5	APP GFLD	DCC	AAP E2	NEO1	FLRT 2	CNTN AP3	SALM 3	FZD6	LRRT M2
J	CDH2	Ntng1	PCDH 8	Ntng2	NOD AL	PlxnA 1	DKK3	PlxnA 2	DDR1	PlxnA 3	EPHB 4	PlxnA 4	PCDH B16	PlxnB 1	CLST N2	PlxnB 2	LAYN	PlxnB 3	CREL D1	PlxnC 1
K	CNPY 4	LRRT M4	CAD M2	UNC5 D	LRFN 1	ACHE	LRRC 4B	CAD M1	PCDH B10	SALM 4	FZD4	SDC4	DKK1	FLRT 1	OLFM L1	AMIG O2	GLDN	CAD M3	CDH1	NTNG 1
L	NTRK 2	PlxnD 1	COC H	RGM a	PCDH B2	Sdk1	CLST N3	Sdk2	FZD7	Sema 3A	IL1RA PL1	Sema 3B	LRRC 4C	Sema 3C	EPHA 4	Sema 3D	PCDH B9	Sema 3E	DKK2	Sema 3F
M	CDH R1	NECT IN2	ICAM 2	EPHA 2	FZD8	EPHA 1	LRRT M3	EPHA 3	LGI3	EPHA 6	TCTN 3	EPHA 7	NCA M1	EPHA 8	FZD1 0	SDK1	CAD M3	TNFR SF1b	ELFN 1	GABB R1α
N	FETU B	Sema 3G	LRRC 70	Sema 4A	NXPE 3	Sema 4B	PCDH B11	Sema 4C	TSPE AR	Sema 4D	PCDH B14	Sema 4F	GPR3 7	Sema 4G	NLGN 2	Sema 5A	NLGN 3	Sema 5B	NLGN 4X	Sema 6A
O	LGI1	GABB R1β	PCDH B5	GABB R2	IGSF 9	FZD1	HEPA CAM	FZD2	PGLY RP3	FZD3	SERP INI1	FZD4	LRFN 3	FZD5	PCDH B6	FZD6	SPON 1	FZD7	FZD5	FZD8
P	LPHN 3	Sema 6B	FLRT 3	Sema 6C	SOR CS1	Sema 6D	LRRT M2	Sema 7A	PTPδ	Unc5 A	SLITR K3	Unc5 B	FNDC 5	Unc5 C	NRXN 1 +4	Unc5 D	NRXN 1b	---	NRXN 2b1	+++

Table S2. Candidate cell adhesion molecules in the ELISA screening, related to Figure 5

NRG3	1	2	3	4	5	6	7	8	9	10	11	12	13	14	15	16	17	18	19	20
A	1.20	1.51	2.43	1.80	2.10	1.87	1.13	2.07	0.98	1.70	2.60	6.07	1.05	3.70	2.07	1.11	2.80	3.02	2.02	3.31
B	1.85	1.06	1.14	1.10	1.00	1.10	1.41	1.21	1.65	1.63	1.52	1.51	1.48	1.45	1.72	1.21	1.58	1.11	1.99	22.31
C	4.19	1.20	1.80	1.20	1.05	1.68	1.85	1.32	15.17	1.05	1.26	1.22	1.02	1.45	1.42	1.55	2.91	3.96	1.53	1.23
D	1.25	1.15	1.43	1.05	1.34	1.35	1.56	1.23	2.17	1.23	1.76	1.03	1.71	1.35	1.44	1.29	1.57	1.14	1.34	1.21
E	1.12	1.58	1.19	1.41	1.19	1.40	1.89	2.30	1.06	1.06	1.09	1.05	1.47	1.58	1.30	1.26	0.96	1.57	1.28	2.04
F	1.14	1.16	0.95	1.05	0.93	1.05	1.17	1.10	1.43	1.42	1.84	1.16	2.12	1.51	2.76	1.24	1.48	1.14	1.69	1.45
G	1.44	1.46	1.20	1.33	1.13	1.37	1.66	1.12	1.08	1.28	3.24	1.48	1.64	1.69	1.97	1.28	2.02	1.12	2.11	1.12
H	1.17	1.14	1.05	6.90	1.11	0.96	0.99	1.54	1.37	3.74	1.84	1.66	2.30	2.46	1.83	1.34	1.67	1.94	1.46	1.89
I	1.27	1.05	1.14	0.99	1.04	1.00	1.17	1.10	1.17	1.34	2.79	16.58	1.34	1.67	1.11	1.39	5.76	1.24	1.95	1.82
J	1.51	1.03	0.93	1.21	1.29	1.02	1.40	1.41	1.44	1.20	1.60	1.40	1.80	1.78	1.88	1.24	1.74	2.22	1.56	1.98
K	1.21	3.27	1.33	1.13	1.23	1.04	1.94	1.47	1.52	1.90	1.36	2.33	2.62	2.04	2.78	1.33	1.93	1.30	1.64	0.97
L	1.74	1.06	1.64	0.96	1.30	1.81	1.63	22.08	1.49	3.23	1.12	1.25	1.19	1.94	1.85	2.38	1.27	2.43	13.08	4.00
M	1.78	1.12	1.29	1.09	1.54	0.95	1.75	1.24	1.04	1.11	1.10	1.58	2.05	1.78	2.40	1.41	2.89	1.27	2.14	4.58
N	1.20	1.38	2.06	2.44	1.68	1.12	2.45	1.56	1.24	1.63	1.58	2.24	2.19	2.43	1.64	1.47	20.07	2.28	1.51	2.04
O	1.18	1.11	1.67	1.27	1.68	1.02	2.31	2.33	2.04	2.16	2.20	1.32	2.35	1.21	2.75	1.89	1.78	1.61	1.29	2.49
P	2.54	1.65	1.41	1.30	1.44	1.39	4.29	1.30	1.34	1.72	1.99	6.29	1.44	7.15	2.18	5.40	1.43	1.62	1.41	22.78

Table S3. OD_{650} data of the ELISA in the screening for binding partners of NRG3, related to Figure 5. Purple cells represent non-specific bindings, which could be detected in negative control tests. Red cells are ErbB4 and Caspr3 wells.

Gene ID	Forward Primer	Reverse Primer
Nrg3	5-TTACG CTGTAGCGACTGCATC-3	5-GCCTA CCACG ATCCA TTTAA GC-3
TH	5-GTCTCAGAGCAGGATACCAAGC-3	5-CTCTCCTCGAATACCACAGCC-3
DAT	5-AAATGCTCCGTGGGACCAATG-3	5-GTCTCCCGCTCTTGAACCTC-3
Bassoon	5'-CAGCACAGGGAGAAACGTTGA-3	5- CAGTAAACAGGCGGGCTGAG-3
Drd1	5-ATGGCTCCTAACACT TCTACCA-3	5-GGGTATTCCCTAAGAGAGTGGAC-3
Cdh2	5-AGCGCAGTCTTACCGAAGG-3	5-TCGCTGCTTTCATACTGAACTTT-3
ERBB4	5-GTGCTATGGACCCTACGTTAGT-3	5-TCATTGAAGTTCATGCAGGCAA-3
Flrt1	5-GATGTGAGTGTGGCCTGGAA-3	5-CAGAGTGTGCCACCACCAT-3
Ncam1	5-CAGGCTCCTGCTAACTCTTCC-3	5-GCACTGGGTT CCCCTTTAGAC-3
Nlgn2	5-ATTCCTCAACTACGACATGCTCA-3	5- GTTGGAGACG GTGAAGTCAAA-3
Nrg1	5-TTCCCATTCTGGCTTGTCTAGT-3	5-CCAGGGTCAAGGTGGGTAG-3
Nrg2	5- GGAGGGCAAGGTACAGGGA-3	5-AGGCTGTCTTAAAAACTAAGGGC-3
Nrxn1	5- AGGACTGCAGCCAAGAAGAC-3	5-TCAGATCCCTTGAACGTGGC-3
Nrxn3	5- TCTACAGCCAGCATTCAGCC-3	5-GCATGTGCTTTGTAGCCACC-3
Rims1	5- CAAACCCTAGCCACCCCAG-3	5-CAGGTGTAGATTTGGAGCCA G -3
Rims2	5- CAATTTGAGACGTTGCGCCAG-3	5-TTGCATTGTTCAGCG TTTGTC-3
Cadm1	5- AGTGATTGGTGGCGTCGTAG-3	5-ATCGGCTCCTTTGGCTTCAT-3
Tenm1	5- CTCCAACCAGCACACAGGAT-3	5-CTGACTGGCTGCACTGAAGA-3
Tenm2	5- CGGGACCTGTAAAGATGGCA-3	5-AGCTGTTCTGACCCAGTGTG-3
Ephb1	5-GAGCTTTGGGCCTCTTACTAGG-3	5-CGATGCTGGGACACTTTTTGAA-3
Ntn1	5-GAGAACGAAGACGACTCGGAG-3	5-GCCGTGTTGTGCCTACAGT-3
Drd2	5-ACCTGTCCTGGTACGATGATG-3	5-GCATGGCATAGTAGTTGTAGTGG-3
Gapdh	5-AAGGTCATCCCAGAGCTGAA-3	5-CTGCTTCACCACCTTCTTGA-3

Table S4. Primers of cell adhesion molecules in the analysis of mRNA from brain tissue and DA neurons, related to STAR Methods.